Journal of Neonatal Surgery
ISSN(Online): 2226-0439
Vol.15 , Issue 1s (2026)
https://www.jneonatalsurg.com

OPEN ACCESS

Synthesis, Characterization, and Biological Evaluation of Novel Benzimidazole Derivatives as Potent Antifungal Agents.

Shaikh Habiburrahman[1], Tejasvinee Sahebrao Chaudhari[2], Swati Anil Mahajan[3], Utkarsh Mahesh Patil[4], Saeed Ahmad[5]*.

[1] Assistant Professor, Department of Pharmaceutical Chemistry, Dr. Uttamrao Mahajan College of Pharmacy, Chalisgaon, Maharashtra, India.

[2] Student, Department of Pharmaceutical Chemistry, Dr. Uttamrao Mahajan College of Pharmacy, Chalisgaon, Maharashtra, India.
(tejasvineechaudhari70@gmail.com)

[3] Student, Department of Pharmaceutical Chemistry, Dr. Uttamrao Mahajan College of Pharmacy, Chalisgaon, Maharashtra, India.

[4] Student, Department of Pharmaceutical Chemistry, Dr. Uttamrao Mahajan College of Pharmacy, Chalisgaon, Maharashtra, India.

[5] Assistant Professor, Department of Pharmaceutics, Dr. Uttamrao Mahajan College of Pharmacy, Chalisgaon, Maharashtra, India.

Corresponding Author:

Tejasvinee Sahebrao Chaudhari

Student, Department of Pharmaceutical Chemistry, Dr. Uttamrao Mahajan College of Pharmacy, Chalisgaon, Maharashtra, India.

Email: tejasvineechaudhari70@gmail.com

Cite this paper as: Shaikh Habiburrahman, Tejasvinee Sahebrao Chaudhari, Swati Anil Mahajan, Utkarsh Mahesh Patil, Saeed Ahmad (2026) Synthesis, Characterization, and Biological Evaluation of Novel Benzimidazole Derivatives as Potent Antifungal Agents... Journal of Neonatal Surgery, 15, (1s) 142-180

ABSTRACT

The present study describes the design, synthesis, and biological evaluation of ten novel 1-acylbenzimidazole derivatives (T1–T10) bearing a 4-((3-hydroxyphenyl) amino)phenyl methanone scaffold with structurally diverse substituents at the 2-position of the benzimidazole ring, developed as potential antifungal, antimicrobial and antioxidant agents. Prior to synthesis, all designed compounds were screened through in silico drug-likeness assessment, ADME prediction, toxicity profiling, and molecular docking against Lanosterol 14α-Demethylase (CYP51, PDB ID: 5FSA), a validated antifungal target involved in fungal ergosterol biosynthesis. All derivatives satisfied Lipinski's Rule of Five with only a single violation, demonstrated favorable pharmacokinetic profiles, and returned inactive predictions across all toxicity endpoints, contrasting favorably with the hepatotoxic liability flagged for the reference drug posaconazole. Molecular docking revealed that compound T3 exhibited the highest binding affinity with a docking score of −7.90 kcal/mol, involving hydrogen bonding, halogen bonding, electrostatic, and hydrophobic interactions with key active site residues. All ten compounds were synthesized via a two-step route using Na_3AlF_6-catalyzed condensation followed by N-acylation, and characterized by FTIR, ^1H NMR, and mass spectrometry. Biological evaluation demonstrated that T3 surpassed ciprofloxacin against Staphylococcus aureus and exceeded posaconazole against Candida albicans at 100 µg/mL, while T4 exhibited the strongest antioxidant activity in both DPPH and ABTS assays. These findings establish T3 as a promising lead compound warranting further pharmacological development..

Keywords: Benzimidazole, Antifungal, Antimicrobial, Antioxidant, Molecular docking, CYP51, Lanosterol 14α-Demethylase, ADME, Drug-likeness, Structure-activity relationship.

INTRODUCTION

1.1.1 Infectious Diseases: Fungal and Bacterial Infections

1.1.2 Global Epidemiology and Burden of Fungal Infections

Infectious diseases have remained one of the foremost threats to human health throughout recorded history

and despite remarkable advances in modern medicine, their burden continues to grow in ways that challenge both clinical practice and public health systems. Among the various categories of infectious disease, fungal infections have emerged as a particularly pressing concern over the past three decades, transforming from conditions historically associated with superficial skin ailments into life-threatening systemic diseases capable of causing widespread mortality across diverse patient populations. The scale of the problem is enormous. A landmark systematic review published in The Lancet Infectious Diseases in 2024, which synthesized data from over 120 countries and drew upon more than 85 published burden studies, estimated that approximately 6.55 million people develop invasive fungal infections every year, leading to a combined death toll of approximately 3.75 million annually, of which 2.55 million deaths are directly attributable to the fungal disease itself. These figures represent a near doubling of prior estimates from the early 2010s and reflect the combined effects of a growing immune compromised population, limited diagnostic capacity in resource-poor settings, and a dangerously narrow therapeutic arsenal.

Among the individual fungal pathogens, Candida species collectively represent the most clinically important group in terms of bloodstream infections and hospital-acquired disease. Candida albicans, in particular, has historically dominated as the primary causative species of invasive candidiasis, a condition encompassing Candida bloodstream infection, deep-seated tissue invasion, and septic shock. The 2024 global burden analysis estimated that approximately 1.565 million people develop Candida bloodstream infections or invasive candidiasis each year, with nearly 995,000 deaths resulting from these infections, translating to a case fatality rate of approximately 63.6%. This level of mortality is comparable to or exceeds that of many advanced malignancies, underscoring the seriousness of invasive candidiasis as a clinical entity. The problem is compounded by the fact that fungal infections are frequently misdiagnosed or diagnosed late, particularly in low- and middle-income countries where laboratory mycology infrastructure is limited. The World Health Organization recognised the gravity of the situation in October 2022 by publishing its first-ever Fungal Priority Pathogens List, which categorised 19 fungal entities into three priority groups critical, high, and medium based on their mortality burden, antifungal resistance trends, global distribution, and the adequacy of available research and treatment tools. Candida species, including *C. albicans, C. auris, C. glabrata, C. tropicalis*, and *C. parapsilosis*, were placed in the critical and high priority categories, reflecting their outsized contribution to global morbidity and mortality.

Beyond Candida, other significant fungal pathogens contributing to the global burden include Aspergillus fumigatus, which causes invasive aspergillosis primarily in patients with haemato logical malignancies or those receiving immunosuppressive therapy, Cryptococcus neoformans, responsible for cryptococcal meningitis predominantly in HIV-positive individuals, and the endemic dimorphic fungi such as Histoplasma capsulatum and Coccidioides immitis. Invasive aspergillosis affects over two million people annually with a crude mortality exceeding 85%, while chronic pulmonary aspergillosis affects an estimated 1.84 million individuals with approximately 340,000 deaths each year. Taken together, the global fungal infection landscape presents an overwhelming clinical challenge that is growing rather than receding, driven by the increasing use of immunosuppressive therapies, broader uptake of organ transplantation, rising incidence of haematological cancers, expanded HIV burden in sub-Saharan Africa, and the growing use of invasive medical devices and broad-spectrum antibacterial agents that disrupt normal microbial flora and create ecological niches for fungal colonisation and infection .

Epidemiology and Clinical Significance of Bacterial Infections

While fungal infections have gained increasing attention, bacterial infections remain the single largest infectious cause of morbidity and mortality globally. Staphylococcus aureus occupies a uniquely prominent position among bacterial pathogens in both community and healthcare settings. It is a Gram-positive, facultative anaerobic coccus that colonises the anterior nares of approximately 30% of the general healthy population and the skin of many individuals without causing disease. However, when host defences are breached through surgical wounds, intravenous catheter placement, trauma, or immunosuppression *S. aureus* demonstrates a remarkable capacity to

establish serious and life-threatening infections including skin and soft tissue infections, wound infections, pneumonia, endocarditis, osteomyelitis, septic arthritis, and bacteremia. Staphylococcal bacteremia carries a 30-day mortality of approximately 15 to 30%, and when complicated by endocarditis or metastatic infection, mortality can exceed 40%. The global incidence of *S. aureus* bacteria is estimated at approximately 150,000 cases per year in Europe alone, with similar burdens documented across North America, Asia, and sub-Saharan Africa .

The clinical significance of *S. aureus* is further amplified by the widespread emergence of antibiotic-resistant strains, most notably methicillin-resistant Staphylococcus aureus (MRSA), which has complicated treatment since the 1960s and now accounts for a substantial proportion of hospital-acquired *S. aureus* infections worldwide. The mechanisms of resistance in MRSA involve acquisition of the mecA gene encoding a modified penicillin-binding protein (PBP2a) with reduced affinity for beta-lactam antibiotics, effectively rendering the entire class of beta-lactam drugs clinically ineffective. Beyond MRSA, vancomycin-intermediate and vancomycin-resistant *S. aureus* (VISA and VRSA) strains have also been described, further narrowing treatment options. The World Health Organization has classified *S. aureus* particularly MRSA as a high-priority pathogen for which new antibacterial agents are urgently needed. The co-existence of *S. aureus* infections alongside fungal infections is particularly concerning in intensive care unit patients, where polymicrobial infections involving both organisms

are associated with significantly worse outcomes than single-pathogen infections. This epidemiological reality makes dual-spectrum antimicrobial agents capable of inhibiting both fungal and bacterial targets particularly valuable and clinically relevant as a research and development goal.

Pathophysiology of *Candida albicans* Infections

The pathophysiology of *Candida albicans* infection is rooted in its remarkable ability to transition between commensal and pathogenic states depending on the balance between host immune defence and fungal virulence factors. *C. albicans* normally resides in the gastrointestinal tract, oral cavity, and vaginal mucosa as a commensal organism, kept in check by competition with bacterial flora, physical mucosal barriers, and innate immune surveillance. Disruption of any of these protective mechanisms through antibiotic therapy, immunosuppression, mucosal trauma, or invasive medical procedures allows *C. albicans* to proliferate, adhere to host tissues, and transition from its yeast form to a filamentous hyphal or pseudohyphal form that is significantly more virulent

.

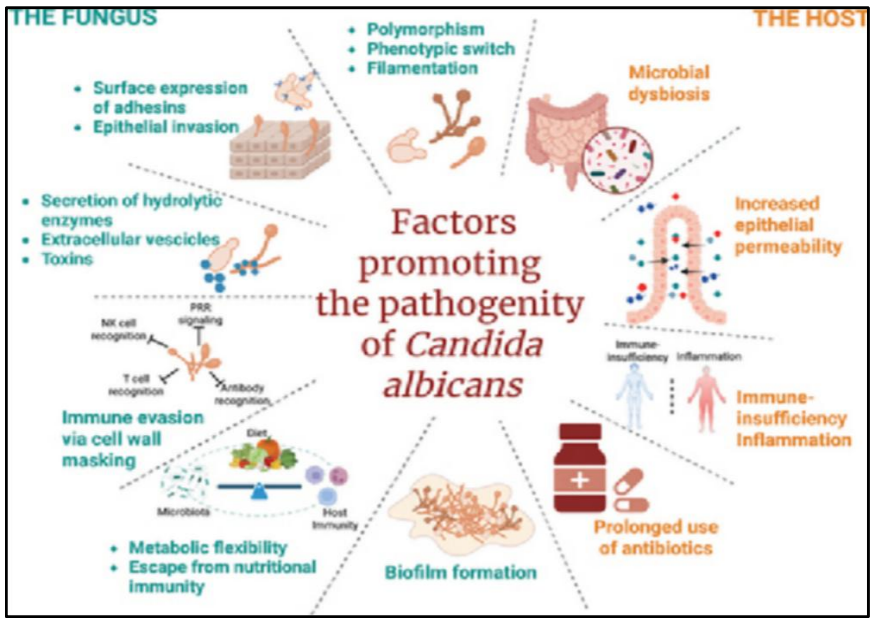

Figure 1: Factors affecting pathogenity of *Candida albicans*

The yeast-to-hypha transition is one of the most critical virulence determinants in C. albicans, as hyphal growth enables tissue penetration, evasion of phagocytic killing by macrophages and neutrophils, and deeper invasion into host organs. Hyphae secrete a range of hydrolytic enzymes including secreted aspartyl proteases (SAPs), phospholipases, and lipases, which degrade host cell membranes, extracellular matrix components, and immunoglobulins, facilitating invasive spread. Another critical virulence factor is the ability of *C. albicans* to form biofilms on both biotic surfaces such as mucosal epithelium and abiotic surfaces such as catheters, prosthetic valves, and implanted medical devices. Biofilm formation dramatically increases resistance to antifungal drugs often by 100- to 1000-fold compared to planktonic cells due to the physical barrier presented by the extracellular matrix, reduced metabolic activity of cells in the biofilm interior, and up regulation of efflux pump gene expression within the biofilm state. The ergosterol biosynthesis pathway is a primary target of antifungal therapy in C. albicans. Ergosterol serves as the functional equivalent of cholesterol in Fungal cell membranes, maintaining membrane fluidity, permeability, and structural integrity. Its depletion through pharmacological inhibition of CYP51 leads to the accumulation of toxic sterol intermediates, impaired membrane function, altered membrane-associated enzymatic activities, and ultimately cell death. This mechanistic pathway is what makes CYP51 the principal validated target for azole-class antifungal drugs, and it is the same target exploited in the present research study.

Current Treatment Strategies and Their Limitations

The current pharmacological treatment of invasive fungal infections rests on three main classes of antifungal agents: the polyenes (primarily amphotericin B and its lipid formulations), the azoles (fluconazole, itraconazole, voriconazole, posaconazole, and isavuconazole), and the echinocandins (caspofungin, micafungin, and anidulafungin). Each class carries distinct mechanisms of action, spectra of activity, and toxicity profiles, and each is associated with meaningful clinical limitations. Amphotericin B, the oldest and broadest-spectrum antifungal agent, acts by binding ergosterol in the fungal cell

membrane and forming pores that disrupt membrane integrity. While highly effective against a wide range of fungi, conventional amphotericin B deoxycholate is associated with severe infusion-related toxicity and dose-limiting nephrotoxicity, which has led to the development of lipid formulations that are better tolerated but substantially more expensive. The echinocandins inhibit β-1,3-glucan synthase, disrupting cell wall integrity, and are generally well-tolerated with activity against most Candida and Aspergillus species. However, echinocandin-resistant Candida strains have been increasingly documented, driven by FKS gene mutations, and the echinocandins lack oral bioavailability, necessitating intravenous administration . The azole antifungals, which are the most widely used class globally due to their oral bioavailability and broad spectrum, act by inhibiting CYP51 and depleting ergosterol. However, the long-term and widespread use of azoles has been accompanied by a growing problem of resistance, driven by several overlapping mechanisms. Overexpression of efflux pumps belonging to the CDR and MDR families actively expels azole molecules from fungal cells, reducing intracellular drug concentrations. Point mutations in the ERG11 gene (which encodes CYP51 in Candida) reduce the affinity of the enzyme for azole drugs, allowing ergosterol synthesis to continue in the presence of drug concentrations that would normally be inhibitory. Additionally, upregulation of the ERG11 gene itself increases the amount of CYP51 enzyme, effectively saturating the drug. Tandem repeat insertions in the CYP51A promoter, combined with coding mutations such as L98H and M220K, have been particularly well-documented in azole-resistant Aspergillus fumigatus isolates and are increasingly found in Candida species as well. Beyond resistance, existing azoles carry safety issues including QT prolongation, hepatotoxicity, visual disturbances, and significant potential for drug-drug interactions through their inhibition of host CYP2C9, CYP2C19, and CYP3A4 enzymes. The bacterial treatment landscape faces an analogous crisis, with increasing resistance among *S. aureus* strains and a dwindling pipeline of new antibacterial agents. These limitations collectively define the scientific context that motivates the search for new chemical entities particularly from well-validated heterocyclic scaffolds that can overcome resistance, improve safety, and broaden therapeutic options for patients with serious fungal and bacterial infections.

Pharmacological Activities of Benzimidazole Derivatives

The pharmacological landscape of benzimidazole derivatives is remarkably broad, encompassing virtually every major disease category addressed by modern medicine. This breadth reflects both the privileged scaffold characteristics of the benzimidazole ring and the extensive medicinal chemistry effort directed at this scaffold over the past six decades. Among the most clinically established applications, the proton pump inhibitors omeprazole, lansoprazole, pantoprazole, and esomeprazole are benzimidazole-based drugs that irreversibly inhibit the gastric H^+/K^+-ATPase enzyme, representing the cornerstone of treatment for peptic ulcer disease, gastroesophageal reflux disease, and Helicobacter pylori eradication. These are among the most widely prescribed drugs in the world, demonstrating the real-world clinical impact of the benzimidazole scaffold. In the antiparasitic field, benzimidazole derivatives including mebendazole, albendazole, thiabendazole, and fenbendazole have long been used as anthelmintics that inhibit tubulin polymerisation in parasitic nematodes and cestodes, interfering with microtubule assembly and disrupting cellular functions essential for parasite survival [33]. Albendazole and mebendazole are WHO essential medicines for soil-transmitted helminths and are among the most widely used drugs globally.

In oncology, numerous benzimidazole derivatives have demonstrated anticancer activity through mechanisms including topoisomerase inhibition, tubulin disruption, kinase inhibition, and induction of apoptosis. Thiabendazole and albendazole have been repurposed as anticancer agents in preclinical and early clinical studies. In the cardiovascular field, telmisartan is an angiotensin II receptor blocker with a benzimidazole core that is widely used in the management of hypertension and heart failure. Antiviral activities of benzimidazole derivatives have been reported against herpes simplex virus, cytomegalovirus, human rhinovirus, and more recently SARS-CoV-2, while antidepressant, anticonvulsant, anti-inflammatory, antidiabetic, and neuroprotective properties have all been documented for variously substituted benzimidazoles. This extraordinary spectrum of pharmacological activities across multiple disease areas is the defining characteristic of the privileged scaffold concept As applied to benzimidazole and provides strong justification for its continued exploration in the discovery of novel antimicrobial and antioxidant agents [34].

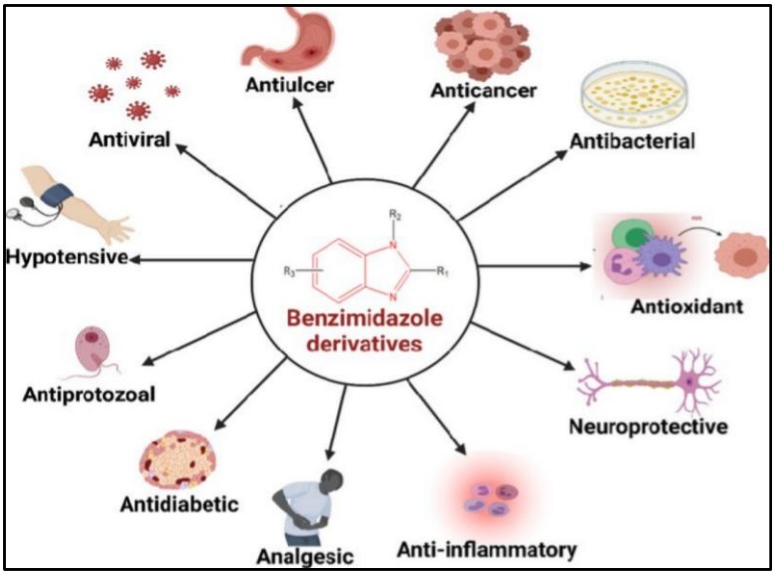

Figure 2: Pharmacological activities of Benzimidazole Derivatives

Structure-Activity Relationships of Benzimidazole Derivatives

A thorough understanding of the structure-activity relationships governing the biological activities of benzimidazole derivatives is essential for rational drug design and for interpreting the pharmacological outcomes of structural variation. The three primary positions available for chemical modification in benzimidazole derivatives are N-1, C-2, and the C-4 through C-7 positions on the benzo ring (equivalent to C-5 and C-6 by conventional numbering when the ring is symmetrically substituted). Each of these positions influences biological activity in characteristic ways that have been systematically documented across numerous published SAR studies.

Substitution at C-2 has the most profound influence on the antimicrobial and antifungal activities of benzimidazole derivatives. The C-2 position connects directly to the imidazole nitrogen lone pairs through conjugation, meaning that substituents at this position significantly modulate the electron density of the entire ring system and Influence its capacity for metal coordination hydrogen bonding, and electrostatic interactions with biological targets. Electron-withdrawing groups at C-2 including halogens such as fluorine and chlorine, trifluoromethyl groups, cyano groups, and nitro groups increase the acidity of the N-H group and enhance the Lewis acid character of the N-3 nitrogen, improving coordination with the heme iron of CYP51 in a manner analogous to the mechanism of azole antifungals. Several published studies have confirmed that fluorinated derivatives, particularly those bearing 4-fluorophenyl or 4-(trifluoromethyl)phenyl substituents at C-2, demonstrate superior antifungal activity compared to unsubstituted or electron-donating substituted analogues, likely due to the combination of improved CYP51 binding and enhanced lipophilicity that facilitates fungal membrane penetration. Electron-donating groups such as methoxy, dimethylamino, and hydroxyl substituents at C-2, while generally less potent as antifungal agents, significantly enhance antioxidant activity by providing hydrogen-donating capacity and stabilising the resulting radical through resonance delocalisation. Substitution on the benzo ring at C-5 or C-6 with electron-withdrawing halogens has also been shown to improve antimicrobial potency, and the introduction of polar functional groups at these positions can modulate water solubility and membrane permeability. Acylation at N-1 with various acyl groups introduces conformational rigidity and additional hydrogen-bonding capacity while also fine-tuning lipophilicity, and the combination of N-1 acylation with C-2 aryl substitution has been a productive strategy for generating benzimidazole derivatives with enhanced and more selective biological activities compared to simple 2-arylbenzimidazoles.

Heterocyclic Compounds in Drug Discovery

Importance of Heterocyclic Scaffolds in Medicinal Chemistry

Heterocyclic compounds, defined as cyclic organic molecules containing at least one ring atom that is not carbon most commonly nitrogen, oxygen, or sulfur represent the single most important class of compounds in medicinal chemistry and pharmaceutical drug discovery. A survey of FDA-approved small molecule drugs consistently reveals that approximately 75 to 85% of all pharmacologically active agents contain at least one heterocyclic ring as a core structural element. This extraordinary prevalence reflects the unique combination of properties that heterocyclic rings confer on drug molecules: they provide a rigid, planar or semi-planar three-dimensional framework that positions substituents precisely in space for optimal interaction with biological targets; they offer multiple sites for the introduction of diverse functional groups through rational

synthetic modification; they are frequently capable of forming hydrogen bonds with biological macromolecules through the lone pairs of heteroatoms or through N-H and O-H donors on the ring itself; and they generally exhibit favourable physicochemical properties including adequate water solubility, appropriate lipophilicity, and metabolic stability .

The concept of "privileged scaffolds" in medicinal chemistry, introduced by Evans and colleagues in 1988, captures the observation that certain heterocyclic frameworks appear disproportionately often in bioactive molecules targeting diverse biological receptors and enzymes. A privileged scaffold is one that has demonstrated high-affinity binding to multiple different protein targets, suggesting that its three-dimensional shape, electronic distribution, and hydrogen-bonding pattern are generically complementary to the architectures of biological binding sites. Recognised privileged scaffolds in medicinal chemistry include benzodiazepines, which are the basis of anxiolytic and anticonvulsant drugs; purines, which underpin the pharmacology of anticancer, antiviral, and immunosuppressive agents; indoles, which are central to the pharmacology of serotonin receptor modulators, kinase inhibitors, and numerous natural products; piperazines, extensively used in antipsychotics and antifungals; and benzimidazoles, which form the focus of the current research investigation. The synthetic accessibility of heterocyclic compounds many of which can be efficiently prepared through well-established condensation, cyclisation, and cross-coupling reactions further enhances their utility in drug discovery, allowing systematic structural variation to establish structusre-activity relationships and optimise biological potency, selectivity, and pharmacokinetic performance.

Pharmacological Activities of Benzimidazole Derivatives

The pharmacological landscape of benzimidazole derivatives is remarkably broad, encompassing virtually every major disease category addressed by modern medicine. This breadth reflects both the privileged scaffold characteristics of the benzimidazole ring and the extensive medicinal chemistry effort directed at this scaffold over the past six decades. Among the most clinically established applications, the proton pump inhibitors omeprazole, lansoprazole, pantoprazole, and esomeprazole are benzimidazole-based drugs that irreversibly inhibit the gastric H^+/K^+-ATPase enzyme, representing the cornerstone of treatment for peptic ulcer disease, gastroesophageal reflux disease, and Helicobacter pylori eradication. These are among the most widely prescribed drugs in the world, demonstrating the real-world clinical impact of the benzimidazole scaffold. In the antiparasitic field, benzimidazole derivatives including mebendazole, albendazole, thiabendazole, and fenbendazole have long been used as anthelmintics that inhibit tubulin polymerisation in parasitic nematodes and cestodes, interfering with microtubule assembly and disrupting cellular functions essential for parasite survival. Albendazole and mebendazole are WHO essential medicines for soil-transmitted helminths and are among the most widely used drugs globally. In oncology, numerous benzimidazole derivatives have demonstrated anticancer activity through mechanisms including topoisomerase inhibition, tubulin disruption, kinase inhibition, and induction of apoptosis. Thiabendazole and albendazole have been repurposed as anticancer agents in preclinical and early clinical studies. In the cardiovascular field, telmisartan is an angiotensin II receptor blocker with a benzimidazole core that is widely used in the management of hypertension and heart failure. Antiviral activities of benzimidazole derivatives have been reported against herpes simplex virus, cytomegalovirus, human rhinovirus, and more recently SARS-CoV-2, while antidepressant, anticonvulsant, anti-inflammatory, antidiabetic, and neuroprotective properties have all been documented for variously substituted benzimidazoles. This extraordinary spectrum of pharmacological activities across multiple disease areas is the defining characteristic of the privileged scaffold concept As applied to benzimidazole and provides strong justification for its continued exploration in the discovery of novel antimicrobial and antioxidant agents.

Structure-Activity Relationships of Benzimidazole Derivatives

A thorough understanding of the structure-activity relationships governing the biological activities of benzimidazole derivatives is essential for rational drug design and for interpreting the pharmacological outcomes of structural variation. The three primary positions available for chemical modification in benzimidazole derivatives are N-1, C-2, and the C-4 through C-7 positions on the benzo ring (equivalent to C-5 and C-6 by conventional numbering when the ring is symmetrically substituted). Each of these positions influences biological activity in characteristic ways that have been systematically documented across numerous published SAR studies.

Substitution at C-2 has the most profound influence on the antimicrobial and antifungal activities of benzimidazole derivatives. The C-2 position connects directly to the imidazole nitrogen lone pairs through conjugation, meaning that substituents at this position significantly modulate the electron density of the entire ring system and Influence its capacity for metal coordination, hydrogen bonding, and electrostatic interactions with biological targets. Electron-withdrawing groups at C-2 including halogens such as fluorine and chlorine, trifluoromethyl groups, cyano groups, and nitro groups increase the acidity of the N-H group and enhance the Lewis acid character of the N-3 nitrogen, improving coordination with the heme iron of CYP51 in a manner analogous to the mechanism of azole antifungals. Several published studies have confirmed that fluorinated derivatives, particularly those bearing 4-fluorophenyl or 4-(trifluoromethyl)phenyl substituents at C-2, demonstrate superior antifungal activity compared to unsubstituted or electron-donating substituted analogues, likely due to the combination of improved CYP51 binding and enhanced lipophilicity that facilitates fungal membrane penetration. Electron-donating groups such as methoxy, dimethylamino, and hydroxyl substituents at C-2, while generally less potent as antifungal agents, significantly enhance antioxidant activity by providing hydrogen-donating capacity and stabilising the

resulting radical through resonance delocalisation. Substitution on the benzo ring at C-5 or C-6 with electron-withdrawing halogens has also been shown to improve antimicrobial potency, and the introduction of polar functional groups at these positions can modulate water solubility and membrane permeability. Acylation at N-1 with various acyl groups introduces conformational rigidity and additional hydrogen-bonding capacity while also fine-tuning lipophilicity, and the combination of N-1 acylation with C-2 aryl substitution has been a productive strategy for generating benzimidazole derivatives with enhanced and more selective biological activities compared to simple 2-arylbenzimidazoles.

Benzimidazole Derivatives as Antifungal and Antibacterial Agents

The antifungal potential of benzimidazole derivatives has been recognised since the early clinical use of anthelmintic benzimidazoles, which incidentally demonstrated activity against fungal organisms, but systematic pharmaceutical exploitation of this scaffold for antifungal drug discovery accelerated significantly from the 1990s onward in response to the growing crisis of azole resistance and the need for structurally distinct CYP51 inhibitors. The structural rationale for benzimidazole as an antifungal pharmacophore is well-founded: the imidazole ring within benzimidazole shares the key nitrogen lone pair that, in classical triazole and imidazole antifungals, coordinates with the heme iron of CYP51, displacing water from the sixth coordination position of the iron and blocking substrate access to the active site. The rigid bicyclic benzimidazole framework orients this nitrogen lone pair in a fixed geometry that may provide different binding characteristics from monocyclic imidazoles or triazoles, potentially allowing interaction with CYP51 active site residues that are less accessible to classical azoles and thereby circumventing some resistance mutations .

Numerous research groups have reported benzimidazole derivatives with potent activity against *Candida albicans* and other Candida species, as well as against Aspergillus flavus, Aspergillus niger, and dermatophytes. The most active compounds from these studies typically feature electron-withdrawing aryl substituents at C-2 particularly 4-fluorophenyl, 4-chlorophenyl, 2,4-dichlorophenyl, and 4-(trifluoromethyl)phenyl groups combined with strategically placed polar substituents or N-1 modifications that optimize binding interactions within the CYP51 active site. Molecular docking studies of benzimidazole derivatives against CYP51 crystal structures consistently show that the imidazole/benzimidazole nitrogen coordinates with the heme iron, while the C-2 aryl substituent projects into the hydrophobic substrate-binding tunnel, and additional hydrogen bonds form between the compound's polar groups and active site residues such as GLY65, GLU70, SER74, HIS373, SER412, GLU420, and ASP502.

These interaction patterns are qualitatively similar to those of established azole drugs, validating benzimidazole as a structurally legitimate CYP51 inhibitor scaffold. With respect to antibacterial activity against *S. aureus* and other Gram-positive organisms, benzimidazole derivatives have shown activity primarily through disruption of cell membrane integrity and inhibition of bacterial DNA gyrase and topoisomerase IV, although the precise mechanisms appear to vary with structural class and specific substitution pattern.

2. MATERIALS AND METHODS

2.1 Methods

2.1.1Drug-Likeness and In Silico ADME Prediction

Drug-likeness and in silico ADME (Absorption, Distribution, Metabolism, and Excretion) properties of all designed benzimidazole derivatives (T1–T10) were predicted to assess their oral bioavailability and pharmacokinetic profiles prior to synthesis. The analysis was performed using ForceADME, a web-based computational tool developed by Geinforce Technology Pvt. Ltd., Pune, India (https://geinforce.com/force-adme/). The two-dimensional structures of all designed compounds were drawn using ChemDraw and saved in MOL file format, which were subsequently uploaded to the ForceADME platform for descriptor calculation. Parameters including molecular weight, lipophilicity (LogP), hydrogen bond donor count, hydrogen bond acceptor count, topological polar surface area (TPSA), rotatable bond count, and bioavailability score were computed and evaluated against Lipinski's Rule of Five and Veber's criteria to assess drug-likeness. The predicted ADME descriptors were interpreted to determine the suitability of the designed compounds as potential oral drug candidates before proceeding to synthetic efforts.

2.1.2Selection of Target Receptor

The target protein selected for molecular docking studies was Lanosterol 14α-Demethylase (CYP51), retrieved from the RCSB Protein Data Bank (https://www.rcsb.org/) under the PDB ID: 5FSA. Lanosterol 14α-Demethylase is a cytochrome P450 enzyme (CYP51A1) that catalyses the oxidative removal of the 14α-methyl group from lanosterol, a critical and rate-limiting step in the ergosterol biosynthesis pathway of fungi. Since ergosterol serves as the primary structural component of the fungal cell membrane -analogous to cholesterol in mammalian cells - its depletion leads to impaired membrane integrity, altered permeability, and ultimately fungal cell death. Inhibition of CYP51 therefore represents a well-validated and clinically relevant antifungal mechanism of action, forming the basis of azole class antifungal therapeutics. The benzimidazole scaffold present in the designed derivatives shares structural and electronic similarities with azole-based CYP51 inhibitors, particularly with respect to the nitrogen lone pair capable of coordinating with the heme iron of the CYP51 active site. This

mechanistic rationale, combined with the diverse electron-donating and electron-withdrawing substituents incorporated at the 2-position of the benzimidazole ring in the designed compounds (T1–T10), provided the pharmacological basis for selecting 5FSA as the target receptor for the present docking study.

Figure 3: Crystal ribbon view of Lanosterol 14α-Demethylase is cytochrome P450 enzyme (CYP51A1) (PDB ID: 5FSA

2.1.3Protein Preparation

The three-dimensional crystal structure of Lanosterol 14α-Demethylase (PDB ID: 5FSA) was downloaded from the RCSB Protein Data Bank (https://www.rcsb.org/) in PDB file format. The downloaded structure was imported into Discovery Studio Visualizer version 4.5 for protein preparation and refinement prior to docking. All water molecules present in the crystal structure were removed to eliminate non-structural solvent interference during docking. Heteroatoms (HETATM), including co-crystallized ligands, cofactors, and ions not essential for docking grid definition, were similarly removed from the structure. The cleaned protein structure was carefully inspected for missing residues, chain integrity, and active site geometry to ensure suitability for computational docking. The prepared protein was subsequently saved in PDB file format and used as the receptor input for molecular docking studies.

2.1.4Molecular Docking

Molecular docking of all designed benzimidazole derivatives (T1–T10) against the prepared Lanosterol 14α-Demethylase receptor (PDB ID: 5FSA) was performed using the GeinDock Suite version 2.5.6, a desktop-based molecular docking application developed by Geinforce Technology Pvt. Ltd., Pune,India. (https://geindock.geinforce.com/). The prepared protein (PDB format) and individual ligand files (MOL format) were uploaded into the GeinDock interface for docking setup. The docking grid box was defined based on the binding site occupied by the co-crystallized ligand in the native crystal structure, following the co-crystallized ligand-based grid selection protocol. The grid centre coordinates were set at x = 199.61, y = 14.36, and z = 57.48, with grid box dimensions of 30.0 × 30.0 × 30.0 Å in the x, y, and z directions, respectively, to encompass the complete active site cavity. Protocol validation was performed by re-docking the co-crystallized ligand into the prepared receptor under identical docking parameters; the resulting root mean square deviation (RMSD) value of less than 2.0 Å confirmed the reliability and accuracy of the docking protocol, and the validated grid was subsequently applied for docking of all designed compounds. Docking poses were analysed based on binding energy scores, key interactions with active site residues, and hydrogen bonding patterns to identify compounds with the most favourable binding affinity towards the target enzyme.

Synthesis of benzimidazole derivatives

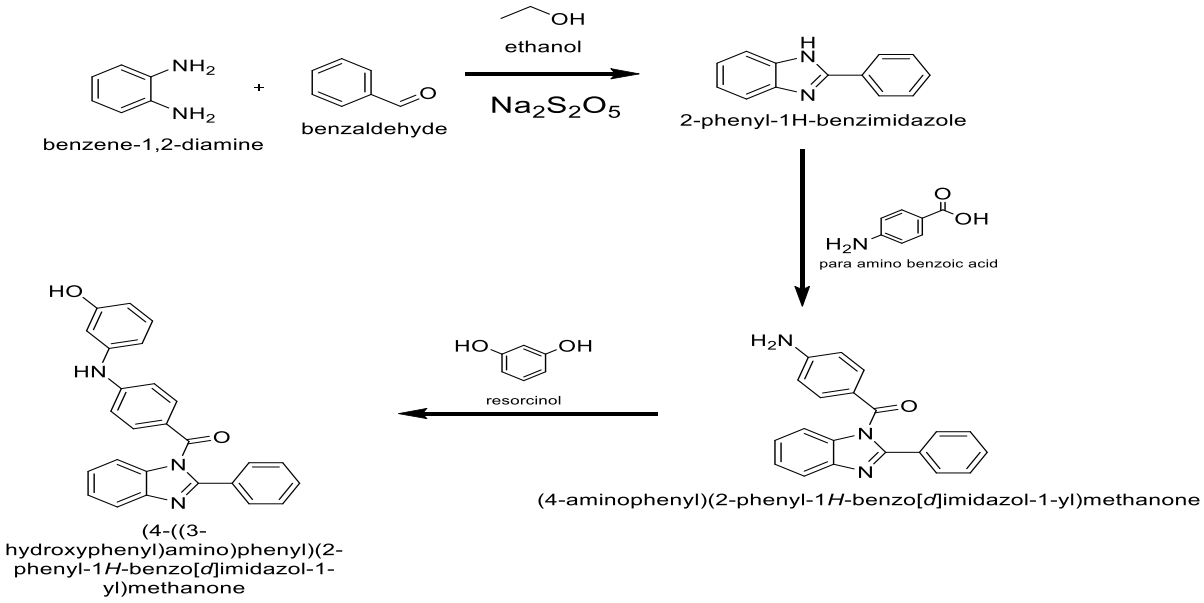

Figure .4:

Proposed scheme for synthesis

Table 1: Derivatives for synthesis of benzimidazole

Label	Structure	IUPAC Name
T1	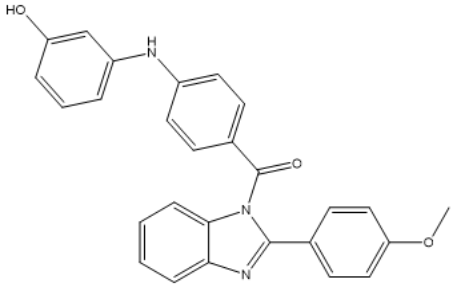	(4-((3-hydroxyphenyl)amino)phenyl)(2-(4-methoxyphenyl)-1H-benzo[d]imidazol-1-yl)methanone
T2	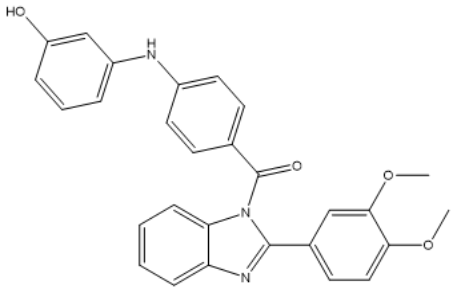	(4-((3-hydroxyphenyl)amino)phenyl)(2-(3,4-dimethoxyphenyl)-1H-benzo[d]imidazol-1-yl)methanone
T3	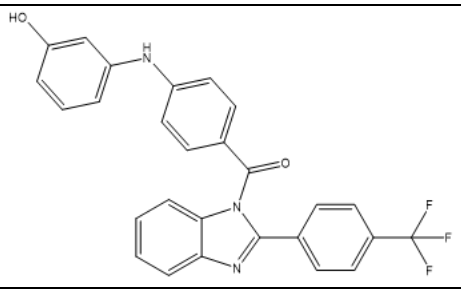	(4-((3-hydroxyphenyl)amino)phenyl)(2-(4-(trifluoromethyl)phenyl)-1H-benzo[d]imidazol-1-yl)methanone

T4	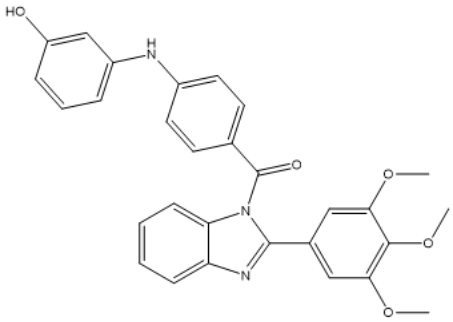	(4-((3-hydroxyphenyl)amino)phenyl)(2-(3,4,5-trimethoxyphenyl)-1H-benzo[d]imidazol-1-yl)methanone
T5	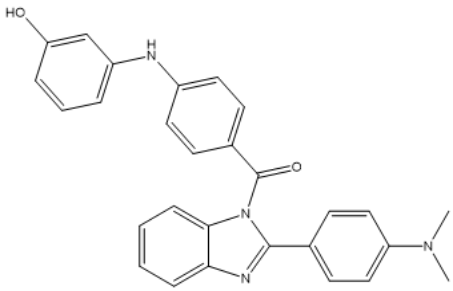	(4-((3-hydroxyphenyl)amino)phenyl)(2-(4-(dimethylamino)phenyl)-1H-benzo[d]imidazol-1-yl)methanone
T6	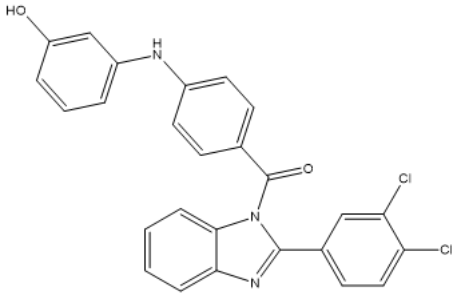	(4-((3-hydroxyphenyl)amino)phenyl)(2-(3,4-dichlorophenyl)-1H-benzo[d]imidazol-1-yl)methanone
T7	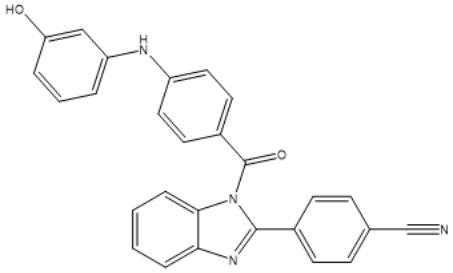	(4-((3-hydroxyphenyl)amino)phenyl)(2-(4-cyanophenyl)-1H-benzo[d]imidazol-1-yl)methanone
T8	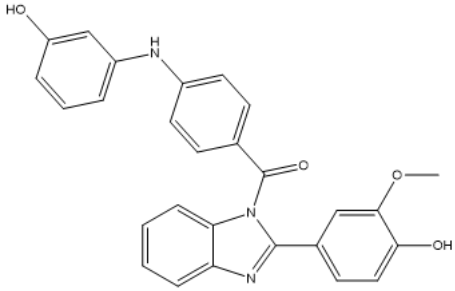	(4-((3-hydroxyphenyl)amino)phenyl)(2-(4-hydroxy-3-methoxyphenyl)-1H-benzo[d]imidazol-1-yl)methanone

T9	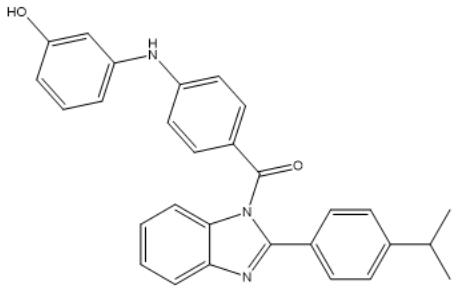	(4-((3-hydroxyphenyl)amino)phenyl)(2-(4-isopropylphenyl)-1H-benzo[d]imidazol-1-yl)methanone
T10	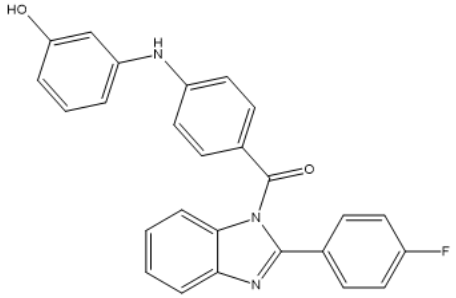	(4-((3-hydroxyphenyl)amino)phenyl)(2-(4-fluorophenyl)-1H-benzo[d]imidazol-1-yl)methanone

Synthesis of benzimidazole derivatives

Synthesis of (4-((3-hydroxyphenyl)amino)phenyl)(2-(4-methoxyphenyl)-1H-benzo[d]imidazol-1-yl)methanone (T1)

In a 100 mL round bottom flask, o-phenylenediamine (1.08 g, 10 mmol) and 4-methoxybenzaldehyde (1.36 g, 10 mmol) were dissolved in absolute ethanol (25 mL) and Na_3AlF_6 (2 mol%, 0.044 g) was added as catalyst. The mixture was stirred at 50°C for 3–4 hours and monitored by TLC using ethyl acetate : n-hexane (3:7 v/v); upon completion, water (30 mL) was added to precipitate the 2-(4-methoxyphenyl)-1H-benzo[d]imidazole intermediate, which was filtered, washed with cold water, and air-dried. In the second step, the intermediate from step 1 (2.24 g, 10 mmol) and 4-((3-hydroxyphenyl)amino)benzoyl chloride (2.76 g, 11 mmol) were dissolved in dry

dichloromethane (25 mL), triethylamine (2.78 mL, 20 mmol) was added, and the mixture was stirred at room temperature for 12 hours; reaction progress was monitored by TLC using ethyl acetate : n-hexane (3:7 v/v), and the product was isolated by washing the organic layer with water (3 × 20 mL), drying over anhydrous Na_2SO_4, and evaporating the solvent under reduced pressure, followed by recrystallization from ethanol.

3.1.3.1 Synthesis o (4-((3-hydroxyphenyl)amino)phenyl)(2-(3,4-dimethoxyphenyl)-1H-benzo[d]imidazol-1-yl)methanone (T2)

In a 100 mL round bottom flask, o-phenylenediamine (1.08 g, 10 mmol) and 3,4-dimethoxybenzaldehyde (1.66 g, 10 mmol) were dissolved in absolute ethanol (25 mL) and Na_3AlF_6 (2 mol%, 0.044 g) was added as catalyst. The reaction mixture was stirred at 50°C for 4–5 hours with TLC monitoring using ethyl acetate : n-hexane (3:7 v/v); after completion, water (30 mL) was added and the precipitated 2-(3,4-dimethoxyphenyl)-1H-benzo[d]imidazole intermediate was filtered, washed with cold water, and air-dried. In the second step, the intermediate from step 1 (2.54 g, 10 mmol) and 4-((3-hydroxyphenyl)amino)benzoyl chloride (2.76 g, 11 mmol) were taken in dry dichloromethane (25 mL), triethylamine (2.78 mL, 20 mmol) was added, and the mixture was stirred at room temperature for 12 hours; the product was isolated by aqueous workup (3 × 20 mL water wash), drying over anhydrous Na_2SO_4, solvent evaporation under reduced pressure, and recrystallization from ethanol.

3.1.3.1 Synthesis of(4-((3-hydroxyphenyl)amino)phenyl)(2-(4-(trifluoromethyl)phenyl)-1H-benzo[d]imidazol-1-yl)methanone (T3)

In a 100 mL round bottom flask, o-phenylenediamine (1.08 g, 10 mmol) and 4-(trifluoromethyl)benzaldehyde (1.74 g, 10 mmol) were dissolved in absolute ethanol (25 mL) and Na_3AlF_6 (2 mol%, 0.044 g) was added. The mixture was stirred at 50°C for 4 hours and monitored by TLC using ethyl acetate : n-hexane (3:7 v/v); water (30 mL) was added after completion to precipitate the 2-(4-(trifluoromethyl)phenyl)-1H-benzo[d]imidazole intermediate, which was filtered, washed with cold water, and air-dried. In the second step, the intermediate from step 1 (2.62 g, 10 mmol) and 4-((3-hydroxyphenyl)amino)benzoyl chloride (2.76 g, 11 mmol) were dissolved in dry dichloromethane (25 mL), triethylamine (2.78 mL, 20 mmol) was added, and the

mixture was stirred at room temperature for 14 hours; the product was isolated by washing with water (3 × 20 mL), drying over anhydrous Na_2SO_4, evaporation under reduced pressure, and recrystallization from ethanol.

3.1..1 Synthesis of(4-((3-hydroxyphenyl)amino)phenyl)(2-(3,4,5-trimethoxyphenyl)-1H-benzo[d]imidazol-1-yl)methanone (T4)

In a 100 mL round bottom flask, o-phenylenediamine (1.08 g, 10 mmol) and 3,4,5-trimethoxybenzaldehyde (1.96 g, 10 mmol) were dissolved in absolute ethanol (25 mL) with Na_3AlF_6 (2 mol%, 0.044 g) as catalyst. The mixture was stirred at 50°C for 5 hours, monitored by TLC using ethyl acetate : n-hexane (3:7 v/v); upon completion, water (30 mL) was added and the precipitated 2-(3,4,5-trimethoxyphenyl)-1H-benzo[d]imidazole intermediate was filtered, washed with cold water, and air-dried. In the second step, the intermediate from step 1 (2.84 g, 10 mmol) and 4-((3-hydroxyphenyl)amino)benzoyl chloride (2.76 g, 11 mmol) were dissolved in dry dichloromethane (25 mL), triethylamine (2.78 mL, 20 mmol) was added, and the mixture was stirred at room temperature for 12 hours; the product was isolated by aqueous workup (3 × 20 mL water wash), drying over anhydrous Na_2SO_4, evaporation under reduced pressure, and recrystallization from ethanol.

Synthesisof(4-((3-hydroxyphenyl)amino)phenyl)(2-(4-(dimethylamino)phenyl)-1H-benzo[d]imidazol-1-yl)methanone (T5)

In a 100 mL round bottom flask, o-phenylenediamine (1.08 g, 10 mmol) and 4-(dimethylamino)benzaldehyde (1.49 g, 10 mmol) were dissolved in absolute ethanol (25 mL) with Na_3AlF_6 (2 mol%, 0.044 g). The reaction mixture was stirred at 50°C for 4 hours with TLC monitoring using ethyl acetate : n-hexane (3:7 v/v); after completion, water (30 mL) was added, and the precipitated 2-(4-(dimethylamino)phenyl)-1H-benzo[d]imidazole intermediate was filtered, washed with cold water, and air-dried. In the second step, the intermediate from step 1 (2.37 g, 10 mmol) and 4-((3-hydroxyphenyl)amino)benzoyl chloride (2.76 g, 11 mmol) were dissolved in dry dichloromethane (25 mL), triethylamine (2.78 mL, 20 mmol) was added, and the mixture was stirred at room temperature for 12 hours; the product was isolated by aqueous workup (3 × 20 mL water wash), drying over anhydrous Na_2SO_4, evaporation under reduced pressure, and recrystallization from ethanol.

Synthesis of (4-((3-hydroxyphenyl)amino)phenyl)(2-(3,4-dichlorophenyl)-1H-benzo[d]imidazol-1-yl)methanone (T6)

In a 100 mL round bottom flask, o-phenylenediamine (1.08 g, 10 mmol) and 3,4-dichlorobenzaldehyde (1.75 g, 10 mmol) were dissolved in absolute ethanol (25 mL) with Na_3AlF_6 (2 mol%, 0.044 g) as catalyst. The mixture was stirred at 50°C for 4 hours, monitored by TLC using ethyl acetate : n-hexane (3:7 v/v); upon completion, water (30 mL) was added and the precipitated 2-(3,4-dichlorophenyl)-1H-benzo[d]imidazole intermediate was filtered, washed with cold water, and air-dried. In the second step, the intermediate from step 1 (2.63 g, 10 mmol) and 4-((3-hydroxyphenyl)amino)benzoyl chloride (2.76 g, 11 mmol) were dissolved in dry dichloromethane (25 mL), triethylamine (2.78 mL, 20 mmol) was added, and the mixture was stirred at room temperature for 14 hours; the product was isolated by aqueous workup (3 × 20 mL water wash), drying over anhydrous Na_2SO_4, evaporation under reduced pressure, and recrystallization from ethanol.

3.1.3.1 Synthesis of (4-((3-hydroxyphenyl)amino)phenyl)(2-(4-cyanophenyl)-1H-benzo[d]imidazol-1-yl)methanone (T7)

In a 100 mL round bottom flask, o-phenylenediamine (1.08 g, 10 mmol) and 4-cyanobenzaldehyde (1.31 g, 10 mmol) were dissolved in absolute ethanol (25 mL) with Na_3AlF_6 (2 mol%, 0.044 g) as catalyst. The reaction was stirred at 50°C for 3–4 hours with TLC monitoring using ethyl acetate : n-hexane (3:7 v/v); after completion, water (30 mL) was added and the precipitated 2-(4-cyanophenyl)-1H-benzo[d]imidazole intermediate was filtered, washed with cold water, and air-dried. In the second step, the intermediate from step 1 (2.19 g, 10 mmol) and 4-((3-hydroxyphenyl)amino)benzoyl chloride (2.76 g, 11 mmol) were dissolved in dry dichloromethane (25 mL), triethylamine (2.78 mL, 20 mmol) was added, and the mixture was stirred at room temperature for 16 hours; the product was isolated by aqueous workup (3 × 20 mL water wash), drying over anhydrous Na_2SO_4, evaporation under reduced pressure, and recrystallization from ethanol.

Synthesis of (4-((3-hydroxyphenyl)amino)phenyl)(2-(4-hydroxy-3-methoxyphenyl)-1H-benzo[d]imidazol-1-yl)methanone (T8)

In a 100 mL round bottom flask, o-phenylenediamine (1.08 g, 10 mmol) and vanillin (4-hydroxy-3-methoxybenzaldehyde, 1.52 g, 10 mmol) were dissolved in absolute ethanol (25 mL) with Na_3AlF_6 (2 mol%, 0.044 g) as catalyst. The mixture was stirred at 50°C for 4–5 hours, monitored by TLC using ethyl acetate : n-hexane (3:7 v/v); upon completion, water (30 mL) was added and the precipitated 2-(4-hydroxy-3-methoxyphenyl)-1H-benzo[d]imidazole intermediate was filtered, washed with cold water, and air-dried. In the second step, the intermediate from step 1 (2.40 g, 10 mmol) and 4-((3-hydroxyphenyl)amino)benzoyl chloride (2.76 g, 11 mmol) were dissolved in dry dichloromethane (25 mL), triethylamine (2.78 mL, 20 mmol) was added, and the mixture was stirred at room temperature for 12 hours; the product was isolated by aqueous workup (3 × 20 mL water wash), drying over anhydrous Na_2SO_4, evaporation under reduced pressure, and recrystallization from ethanol.

Synthesis of (4-((3-hydroxyphenyl)amino)phenyl)(2-(4-isopropylphenyl)-1H-benzo[d]imidazol-1-yl)methanone (T9)

In a 100 mL round bottom flask, o-phenylenediamine (1.08 g, 10 mmol) and 4-isopropylbenzaldehyde (1.48 g, 10 mmol) were dissolved in absolute ethanol (25 mL) with Na_3AlF_6 (2 mol%, 0.044 g) as catalyst. The mixture was stirred at 50°C for 3–4 hours with TLC monitoring using ethyl acetate : n-hexane (3:7 v/v); upon completion, water (30 mL) was added and the precipitated 2-(4-isopropylphenyl)-1H-benzo[d]imidazole intermediate was filtered, washed with cold water, and air-dried. In the second step, the intermediate from step 1 (2.36 g, 10 mmol) and 4-((3-hydroxyphenyl)amino)benzoyl chloride (2.76 g, 11 mmol) were dissolved in dry dichloromethane (25 mL), triethylamine (2.78 mL, 20 mmol) was added, and the mixture was stirred at room temperature for 12 hours; the product was isolated by aqueous workup (3 × 20 mL water wash), drying over anhydrous Na_2SO_4, evaporation under reduced pressure, and recrystallization from ethanol.

Synthesis of (4-((3-hydroxyphenyl)amino)phenyl)(2-(4-fluorophenyl)-1H-benzo[d]imidazol-1-yl)methanone (T10)

In a 100 mL round bottom flask, o-phenylenediamine (1.08 g, 10 mmol) and 4-fluorobenzaldehyde (1.24 g, 10 mmol) were dissolved in absolute ethanol (25 mL) with Na_3AlF_6 (2 mol%, 0.044 g) as catalyst. The mixture was stirred at 50°C for 3–4 hours, monitored by TLC using ethyl acetate : n-hexane (3:7 v/v); upon completion, water (30 mL) was added and the precipitated 2-(4-fluorophenyl)-1H-benzo[d]imidazole intermediate was filtered, washed with cold water, and air-dried. In the second step, the intermediate from step 1 (2.12 g, 10 mmol) and 4-((3-hydroxyphenyl)amino)benzoyl chloride (2.76 g, 11 mmol) were dissolved in dry dichloromethane (25 mL), triethylamine (2.78 mL, 20 mmol) was added, and the mixture was stirred at room temperature for 12 hours; the product was isolated by aqueous workup (3 × 20 mL water wash), drying over anhydrous Na_2SO_4, evaporation under reduced pressure, and recrystallization from ethanol.

4. Result and Discussion

Lipinski's Rule of Five

The drug-likeness of all ten synthesized derivatives was evaluated against Lipinski's Rule of Five and Veber's rule parameters to assess their potential as orally bioavailable drug candidates. All ten compounds exhibited only one violation across the dataset, specifically related to the elevated MLogP values, which ranged from 7.39 to 10.84. While this exceeds the recommended threshold of 5, such higher lipophilicity values are commonly observed in antifungal scaffolds bearing halogenated aromatic systems and extended hydrophobic frameworks, and do not necessarily preclude biological activity or absorption when considered alongside other parameters. Molecular weights of all derivatives fell within a reasonable range of 423.45 to 495.53 g/mol, comfortably below the 500 g/mol cutoff, suggesting favorable passive membrane permeability. Hydrogen bond donor counts were uniformly 2 or 3 across all compounds, and hydrogen bond acceptors ranged from 5 to 8, both well within the acceptable limits. Regarding Veber's rule, TPSA values ranged from 67.15 to 96.61 Å², remaining below the 140 Å² threshold, and rotatable bond counts between 5 and 11 stayed within permissible limits, collectively indicating adequate oral bioavailability potential. In contrast, the standard drug posaconazole exhibited three violations with a molecular weight of 700.79 g/mol, TPSA of 115.7 Å², and 15 rotatable bonds, reinforcing the comparatively favorable drug-likeness profile demonstrated by the synthesized series.

Table .2: Lipinski's Rule of Five and Veber's Rule Parameters for All Compounds

Compound Codes	Lipinski rule of five					Veber's rule	
	M Log P	Mol. Wt. (g/mol)	HBA	HBD	Violations	TPSA (Å^2)	No. of rotatable bonds
T1	8.85	435.48	6	2	1	76.38	7
T2	8.28	465.51	7	2	1	85.61	9
T3	9.94	473.45	5	2	1	67.15	5
T4	7.71	495.53	8	2	1	94.84	11
T5	7.48	448.53	6	2	1	70.39	8
T6	10.84	474.35	5	2	1	67.15	5
T7	7.39	430.47	6	2	1	90.94	5
T8	8.18	451.48	7	3	1	96.61	8
T9	9.72	447.54	5	2	1	67.15	8
T10	9.56	423.45	5	2	1	67.15	5

Posaconzole	-0.84	700.79	12	1	3	115.7	15

Mol. Wt.: Molecular weight; HBA: Hydrogen bond acceptors; HBD: Hydrogen bond donors; TPSA: Total polar surface area

Drug likeness and ADME analysis

The pharmacokinetic profiles of all ten synthesized benzimidazole derivatives were assessed through in silico ADME prediction to understand their absorption, distribution, metabolism, and excretion behavior. All compounds demonstrated low gastrointestinal absorption, which is broadly consistent with their elevated lipophilicity values observed in the Lipinski analysis, as highly lipophilic molecules often face solubility limitations that restrict GI permeation despite favorable membrane partitioning. None of the compounds showed blood-brain barrier penetration, which is a desirable characteristic for antifungal agents where CNS exposure is generally undesirable. Regarding P-glycoprotein substrate activity, compounds T1, T2, T4, T5, T7, and T8 were identified as P-gp substrates, suggesting these may be subject to efflux-mediated reduction in intracellular concentration, while T3, T6, T9, and T10 were non-substrates, potentially offering better cellular retention.

In terms of metabolic liability, all compounds showed inhibitory activity toward CYP1A2 and CYP2C9 enzymes, while none inhibited CYP2D6. CYP2C19 and CYP3A4 inhibition patterns were consistent across the series. Drug-likeness filters including Ghose, Egan, and Muegge were not satisfied by any compound, which is partly attributable to the high lipophilicity of the scaffold. Bioavailability scores of 0.85 were recorded for T1, T3, T6, T7, and T10, indicating relatively better predicted oral bioavailability compared to T2, T4, T5, T8, and T9 which scored 0.55. Notably, posaconazole showed the lowest bioavailability score of 0.17, further highlighting the comparative advantage of the synthesized series.

Table 4.2: Pharmacokinetics and Drug-likeness Properties of benzimidazole derivativs

Comp. codes	Pharmacokinetics									Drug-likeness			
	GI abs.	BBB per.	P-gp sub.	CYP1A2	CYP2C19	CYP2C9	CYP2D6	CYP3A4	Log K_p (skin permeation, cm/s)	Ghose	Egan	Muegge	Bioavailability Score
				inhibitors									
T1	Low	No	Yes	Yes	No	Yes	No	Yes	14.98	No	No	No	0.85
T2	Low	No	Yes	Yes	No	Yes	No	Yes	15.56	No	No	No	0.55
T3	Low	No	No	Yes	No	Yes	No	Yes	15.14	No	No	No	0.85
T4	Low	No	Yes	Yes	No	Yes	No	Yes	16.14	No	No	No	0.55
T5	Low	No	Yes	Yes	No	Yes	No	Yes	15.72	No	No	No	0.55
T6	Low	No	No	Yes	No	Yes	No	Yes	16.03	No	No	No	0.85

T7	Low	No	Yes	Yes	No	Yes	No	Yes	14.5	No	No	No	0.85
T8	Low	No	Yes	Yes	No	Yes	No	Yes	14.87	No	No	No	0.55
T9	Low	No	No	Yes	No	Yes	No	Yes	16.47	No	No	No	0.55
T10	Low	No	No	Yes	No	Yes	No	Yes	14.36	No	No	No	0.85
T1	Low	No	Yes	Yes	No	Yes	No	Yes	14.98	No	No	No	0.85
Posaconazole	Low	No	Yes	Yes	No	Yes	No	Yes	18.89	No	No	No	0.17

GI abs.: Gastrointestinal absorption; BBB per.: Blood brain barrier permeate; P-gp sub.: P-glycoprotein substrate

In Silico Toxicity Prediction

The in silico toxicity profiles of all ten synthesized benzimidazole derivatives were evaluated using GeinTox-II across five critical toxicity endpoints: hepatotoxicity, carcinogenicity, immunotoxicity, mutagenicity, and cytotoxicity. All compounds were classified under Toxicity Class 4, which corresponds to substances considered harmful if swallowed, representing a relatively acceptable acute toxicity category for drugCandidates at the early discovery stage. The LD_{50} values across the series ranged from

423.8 mg/kg for T3 to 845.5 mg/kg for T4 and T8, indicating moderate to reasonable acute toxicity margins. Compounds T4 and T8 demonstrated the highest predicted LD_{50} values of 845.5 mg/kg, suggesting comparatively lower acute toxicity potential within the series, which is a favorable attribute from a safety standpoint.

Across all five toxicity endpoints, every synthesized compound returned inactive predictions with uniformly low probabilities. Hepatotoxicity probabilities ranged narrowly between 0.30 and 0.32, carcinogenicity, immunotoxicity, mutagenicity, and cytotoxicity all recorded probabilities of 0.10 to 0.12, well below the threshold for active classification. This clean toxicity profile across the entire series is particularly encouraging for further development In contrast, the reference drug posaconazole, despite having a higher LD_{50} of 1503.6 mg/kg, was flagged as active for hepatotoxicity with a probability of 0.54, raising concerns about liver-related adverse effects associated with its long-term clinical use. The absence of hepatotoxic liability in all synthesized derivatives therefore represents a meaningful safety advantage over the existing standard drug.

Table 4.3: In Silico Toxicity Prediction of Designed Benzimidazole Derivatives (T1-T10) and Reference Standard (Posaconazole).

Comp.	LD_{50} (mg/ kg)	Toxicity Class	(Probability)				
			Hepatotoxicity	Carcinogenicity	Immunotoxicity	Mutagenicity	Cytotoxicity
T1	533.5	Class 4	Inactive (0.31)	Inactive (0.10)	Inactive (0.10)	Inactive (0.12)	Inactive (0.12)
T2	671.6	Class 4	Inactive (0.31)	Inactive (0.10)	Inactive (0.10)	Inactive (0.12)	Inactive (0.12)
T3	423.	Class	Inactive	Inactive	Inactive	Inactive	Inactive

	8	4	(0.32)	(0.10)	(0.30)	(0.12)	(0.12)
T4	845.5	Class 4	Inactive (0.31)	Inactive (0.10)	Inactive (0.10)	Inactive (0.12)	Inactive (0.12)
T5	533.5	Class 4	Inactive (0.32)	Inactive (0.10)	Inactive (0.10)	Inactive (0.12)	Inactive (0.12)
T6	533.5	Class 4	Inactive (0.32)	Inactive (0.10)	Inactive (0.10)	Inactive (0.12)	Inactive (0.12)
T7	671.6	Class 4	Inactive (0.31)	Inactive (0.10)	Inactive (0.10)	Inactive (0.12)	Inactive (0.12)
T8	845.5	Class 4	Inactive (0.30)	Inactive (0.10)	Inactive (0.10)	Inactive (0.12)	Inactive (0.12)
T9	533.	Class	Inactive	Inactive	Inactive	Inactive	Inactive
	5	4	(0.32)	(0.10)	(0.10)	(0.12)	(0.12)
T10	533.5	Class 4	Inactive (0.32)	Inactive (0.10)	Inactive (0.10)	Inactive (0.12)	Inactive (0.12)
Posacon azole	1503.6	Class 4	Active (0.54)	Inactive (0.10)	Inactive (0.10)	Inactive (0.12)	Inactive (0.12)

Molecular Docking analysis

The molecular docking study of all ten synthesized benzimidazole derivatives was carried out against Lanosterol 14α-Demethylase (CYP51) using the crystal structure deposited under PDB ID: 5FSA to understand their binding behavior and interaction patterns within the active site of this clinically validated antifungal target. Among all derivatives, compound T3 emerged as the most promising candidate with the highest binding affinity, recording a docking score of −7.90 kcal/mol. This compound established a rich network of interactions including two conventional hydrogen bonds with GLN67 and ASP421, two carbon hydrogen bonds with ASP502 and PRO503, a halogen interaction involving GLU70 through its fluorine substituent, multiple pi-anion electrostatic interactions with GLU70, GLU325, GLU420, and ASP502, a pi-donor hydrogen bond with GLN67, and hydrophobic pi-alkyl contacts with PRO503. The diversity and strength of these interactions collectively explain the superior binding affinity of T3 and suggest that the combination of hydrogen bonding capacity, halogen bonding from the fluorine atom, and hydrophobic complementarity within the active site contributes meaningfully to its favorable docking outcome. Compounds T4 and T5 both recorded docking scores of −7.60 kcal/mol, placing them as the second most active pair within the series. T4 interacted through a conventional hydrogen bond with GLY65, a carbon hydrogen bond with HIS373, electrostatic pi-anion interactions with GLU70, GLU420, and ASP502, and extensive hydrophobic contacts with VAL500, PRO503, MET372, TYR69, and HIS373. The involvement of MET372 and HIS373 in hydrophobic contacts is noteworthy, as these residues are located within the hydrophobic substrate-binding channel of CYP51 and their engagement suggests deep pocket penetration by T4. Compound T5, while achieving the same docking score, showed a comparatively simpler interaction profile dominated by a carbon hydrogen bond with HIS373 and three electrostatic pi-anion interactions with GLU420, suggesting its binding is primarily driven by electrostatic complementarity rather than hydrogen bonding. Compounds T6 and T7 scored −7.61 and −7.52 kcal/mol respectively, both engaging SER412 and GLU73 through conventional hydrogen bonds, with additional pi-donor hydrogen bonds involving SER74 and hydrophobic amide-pi stacked interactions with THR411, indicating a shared binding orientation within the active site for this structural subclass. Compounds T1, T8, T9, and T10 demonstrated moderate binding affinities, with T1 scoring −7.38 kcal/mol through three conventional hydrogen bonds with THR196, SER203, and LEU204, along with an alkyl hydrophobic contact with LEU305, reflecting a hydrogen bond-driven binding mode in a distinct region of the active site. Compounds T8, T9, and T10, although their docking scores were not explicitly listed in the data, showed rich interaction profiles involving conventional hydrogen bonds, electrostatic pi-anion interactions with GLU420 and ASP502, and substantial hydrophobic networks engaging residues PRO503, VAL500, TYR498, TYR505, and LYS499, suggestive of favorable active site complementarity. Compound T10 was particularly notable for exhibiting dual halogen bonding interactions with VAL500 and GLU325 in addition to multiple hydrogen bonds and electrostatic contacts, making it structurally interesting for further optimization. In comparison, the reference drug posaconazole recorded a markedly superior docking score of −12.36 kcal/mol with an extensive interaction network spanning 21 contacts including conventional and carbon hydrogen bonds,

halogen interactions, multiple pi-pi stacked and pi-alkyl hydrophobic interactions with key residues such as TYR132, TYR118, TYR64, HIS377, and several leucine and isoleucine residues lining the hydrophobic core. While posaconazole outperformed the synthesized series in docking score, the comparable binding residue engagement and the cleaner toxicity profiles of the synthesized derivatives present them as worthwhile leads for structural refinement and further optimization toward potent CYP51 inhibition.

Table 4.4: Molecular docking interaction analysis of synthesized compounds with Lanosterol 14α-Demethylase (CYP51) (PDB ID: 5FSA)

Active Amino acid	Bond length	Bond Category	Bond Type	Docking score
Compound: T1				
THR196	2.9444	Hydrogen Bond	Conventional Hydrogen	**-7.38**
			Bond	
SER203	3.25784	Hydrogen Bond	Conventional Hydrogen Bond	
LEU204	2.97969	Hydrogen Bond	Conventional Hydrogen Bond	
LEU305	5.12967	Hydrophobic	Alkyl	
Compound: T2				
SER412	2.6153	Hydrogen Bond	Conventional Hydrogen Bond	
GLU70	3.85019	Electrostatic	Pi-Anion	
GLU70	3.47099	Electrostatic	Pi-Anion	
GLU73	3.43793	Electrostatic	Pi-Anion	**-6.65**
GLU413	4.77405	Electrostatic	Pi-Anion	
GLU420	3.34901	Electrostatic	Pi-Anion	
GLU420	3.25831	Electrostatic	Pi-Anion	
L:LIG1	4.28409	Hydrophobic	Pi-Pi Stacked	
Compound: T3				
GLN67	3.3515	Hydrogen Bond	Conventional Hydrogen Bond	
ASP421	2.25128	Hydrogen Bond	Conventional Hydrogen Bond	
ASP502	3.68289	Hydrogen Bond	Carbon Hydrogen Bond	
A:PRO503	2.85187	Hydrogen Bond	Carbon Hydrogen Bond	

GLU70	3.4667	Halogen	Halogen (Fluorine)	**-7.90**
GLU70	3.81311	Electrostatic	Pi-Anion	
GLU325	3.44084	Electrostatic	Pi-Anion	
GLU420	4.43961	Electrostatic	Pi-Anion	
GLU420	3.81187	Electrostatic	Pi-Anion	
ASP502	4.54458	Electrostatic	Pi-Anion	
GLN67	3.9811	Hydrogen Bond	Pi-Donor Hydrogen Bond	
PRO503	4.88548	Hydrophobic	Pi-Alkyl	
PRO503	5.0074	Hydrophobic	Pi-Alkyl	
Compound: T4				
GLY65	2.23041	Hydrogen Bond	Conventional Hydrogen Bond	**-7.60**
HIS373	3.51667	Hydrogen Bond	Carbon Hydrogen Bond	
GLU70	4.33835	Electrostatic	Pi-Anion	
GLU70	4.35353	Electrostatic	Pi-Anion	
GLU420	4.29278	Electrostatic	Pi-Anion	
ASP502	3.44036	Electrostatic	Pi-Anion	
ASP502	4.0902	Electrostatic	Pi-Anion	
VAL500	4.6837	Hydrophobic	Alkyl	
PRO503	4.66422	Hydrophobic	Alkyl	
MET372	4.19465	Hydrophobic	Alkyl	
TYR69	5.0403	Hydrophobic	Pi-Alkyl	
HIS373	5.09354	Hydrophobic	Pi-Alkyl	
PRO503	4.78171	Hydrophobic	Pi-Alkyl	
Compound: T5				
HIS373	3.35952	Hydrogen Bond	Carbon Hydrogen Bond	**-7.60**
GLU420	3.71413	Electrostatic	Pi-Anion	
GLU420	3.86782	Electrostatic	Pi-Anion	
GLU420	3.75061	Electrostatic	Pi-Anion	
Compound: T6				
SER412	3.09241	Hydrogen Bond	Conventional Hydrogen Bond	

GLU73	2.14204	Hydrogen Bond	Conventional Hydrogen Bond	**-7.61**
SER74	3.41291	Hydrogen Bond	Pi-Donor Hydrogen Bond	
THR411	4.55864	Hydrophobic	Amide-Pi Stacked	
ATRP54	4.86341	Hydrophobic	Pi-Alkyl	
Compound: T7				
SER412	3.04011	Hydrogen Bond	Conventional Hydrogen Bond	**-7.52**
GLU73	2.61781	Hydrogen Bond	Conventional Hydrogen Bond	
SER63	3.36523	Hydrogen Bond	Carbon Hydrogen Bond	
GLU70	4.49691	Electrostatic	Pi-Anion	
SER74	4.14393	Hydrogen Bond	Pi-Donor Hydrogen Bond	
TYR69	5.05905	Hydrophobic	Amide-Pi Stacked	
THR411	4.41709	Hydrophobic	Amide-Pi Stacked	
Compound: T8				
A:GLU70	2.113	Hydrogen Bond	Conventional Hydrogen Bond	**-7.52**
HIS373	3.26995	Hydrogen Bond	Carbon Hydrogen Bond	
GLU420	4.27658	Electrostatic	Pi-Anion	
GLU420	3.907	Electrostatic	Pi-Anion	
GLU420	3.72455	Electrostatic	Pi-Anion	
LIG1	4.53262	Hydrophobic	Pi-Pi T-shaped	
PRO503	4.03107	Hydrophobic	Alkyl	
TYR505	5.17417	Hydrophobic	Pi-Alkyl	
VAL500	4.91345	Hydrophobic	Pi-Alkyl	

Compound: T9				
VAL500	2.51462	Hydrogen Bond	Conventional Hydrogen Bond	**-7.52**
ASP502	4.6977	Electrostatic	Pi-Anion	
THR513	3.86657	Hydrophobic	Pi-Sigma	
TYR498	5.08678	Hydrophobic	Pi-Pi T-shaped	
LIG1	4.74519	Hydrophobic	Pi-Pi T-shaped	
TYR498	5.18841	Hydrophobic	Pi-Alkyl	
PRO515	4.74574	Hydrophobic	Pi-Alkyl	
LYS499	3.71582	Hydrophobic	Pi-Alkyl	
PRO501	4.94148	Hydrophobic	Pi-Alkyl	
PRO515	4.78353	Hydrophobic	Pi-Alkyl	
Compound: T10				
VAL500	3.56271	Hydrogen Bond;Halogen	Conventional Hydrogen Bond;Haloge n (Fluorine)	**-7.60**
GLU70	2.28658	Hydrogen Bond	Conventional Hydrogen Bond	
LYS499	3.09043	Hydrogen Bond	Carbon Hydrogen Bond	
A:PRO503	3.52999	Hydrogen Bond	Carbon Hydrogen Bond	
GLU325	3.01769	Halogen	Halogen (Fluorine)	
GLU420	3.49851	Electrostatic	Pi-Anion	
GLU420	3.88879	Electrostatic	Pi-Anion	
ASP502	3.96652	Electrostatic	Pi-Anion	
PRO503	5.00542	Hydrophobic	Pi-Alkyl	

VAL500	4.84431	Hydrophobic	Pi-Alkyl	
Compounds: Posaconazole				
TYR132	2.83713	Hydrogen Bond	Conventional Hydrogen Bond	**-12.36**
SER506	2.53789	Hydrogen Bond	Conventional Hydrogen Bond	
GLY65	3.78213	Hydrogen Bond	Carbon Hydrogen Bond	
SER378	2.5233	Hydrogen Bond	Carbon Hydrogen Bond	
TYR132	2.92527	Hydrogen Bond	Carbon Hydrogen Bond	
ILE304	3.09429	Hydrogen Bond	Carbon Hydrogen Bond	
GLN142	3.51722	Halogen	Halogen (Fluorine)	
TYR118	3.89038	Hydrophobic	Pi-Pi Stacked	
TYR64	5.3785	Hydrophobic	Pi-Pi Stacked	
HIS377	4.65562	Hydrophobic	Pi-Pi T-shaped	
ALA61	3.90433	Hydrophobic	Alkyl	
LEU121	5.44707	Hydrophobic	Alkyl	
LEU376	4.76893	Hydrophobic	Alkyl	
LEU87	5.26002	Hydrophobic	Alkyl	
LEU376	5.49056	Hydrophobic	Pi-Alkyl	
PRO230	5.09433	Hydrophobic	Pi-Alkyl	
ILE304	4.64672	Hydrophobic	Pi-Alkyl	
ILE131	4.83976	Hydrophobic	Pi-Alkyl	
LYS143	5.04045	Hydrophobic	Pi-Alkyl	
LYS499	3.09043	Hydrogen Bond	Carbon Hydrogen Bond	
A:PRO503	3.52999	Hydrogen Bond	Carbon Hydrogen Bond	
GLU325	3.01769	Halogen	Halogen (Fluorine)	

GLU420	3.49851	Electrostatic	Pi-Anion	
GLU420	3.88879	Electrostatic	Pi-Anion	
ASP502	3.96652	Electrostatic	Pi-Anion	
PRO503	5.00542	Hydrophobic	Pi-Alkyl	
VAL500	4.84431	Hydrophobic	Pi-Alkyl	
Compounds: Posaconazole				
TYR132	2.83713	Hydrogen Bond	Conventional Hydrogen Bond	
SER506	2.53789	Hydrogen Bond	Conventional Hydrogen Bond	
GLY65	3.78213	Hydrogen Bond	Carbon Hydrogen Bond	
SER378	2.5233	Hydrogen Bond	Carbon Hydrogen Bond	
TYR132	2.92527	Hydrogen Bond	Carbon Hydrogen Bond	
ILE304	3.09429	Hydrogen Bond	Carbon Hydrogen Bond	
GLN142	3.51722	Halogen	Halogen (Fluorine)	**-12.36**
TYR118	3.89038	Hydrophobic	Pi-Pi Stacked	
TYR64	5.3785	Hydrophobic	Pi-Pi Stacked	
HIS377	4.65562	Hydrophobic	Pi-Pi T-shaped	
ALA61	3.90433	Hydrophobic	Alkyl	
LEU121	5.44707	Hydrophobic	Alkyl	
LEU376	4.76893	Hydrophobic	Alkyl	
LEU87	5.26002	Hydrophobic	Alkyl	
LEU376	5.49056	Hydrophobic	Pi-Alkyl	
PRO230	5.09433	Hydrophobic	Pi-Alkyl	
ILE304	4.64672	Hydrophobic	Pi-Alkyl	
ILE131	4.83976	Hydrophobic	Pi-Alkyl	
LYS143	5.04045	Hydrophobic	Pi-Alkyl	
ILE304	5.22906	Hydrophobic	Pi-Alkyl	
ILE471	5.42346	Hydrophobic	Pi-Alkyl	

Table 4.5: Docking Poses 2D and 3D.

3D-docking poses	2D-docking poses
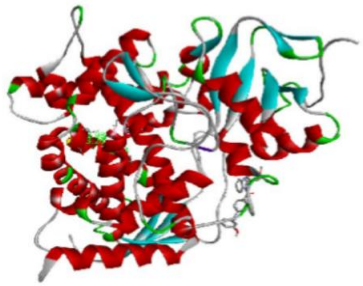	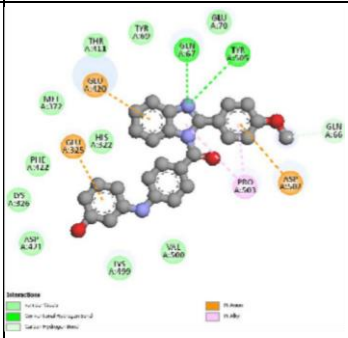
Compound: T1	
	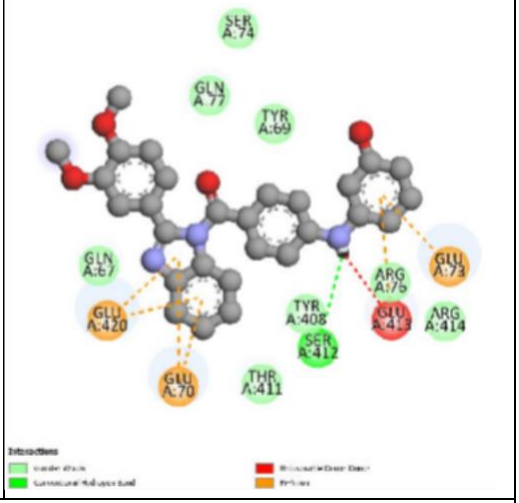
Compound: T2	
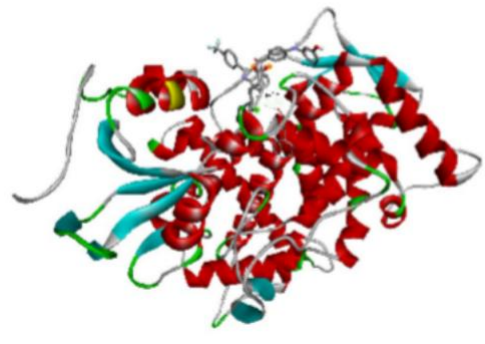	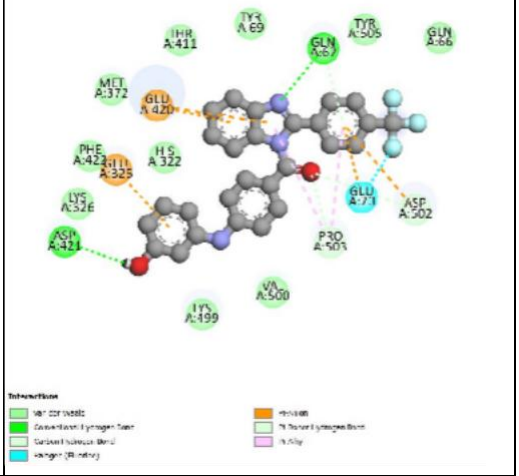
Compound: T3	

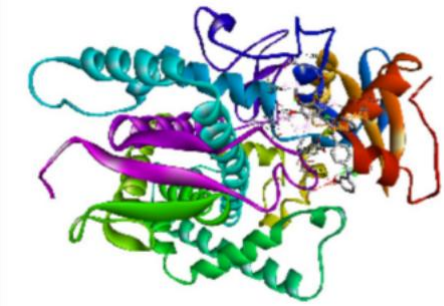

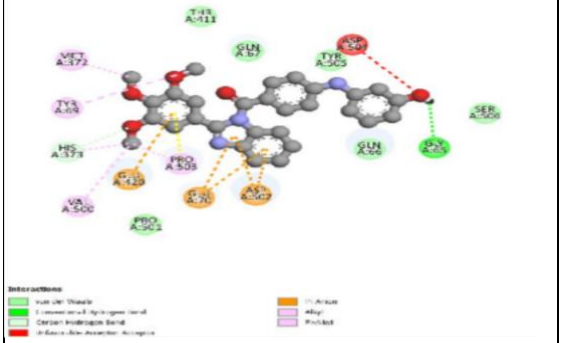

Compound: T4

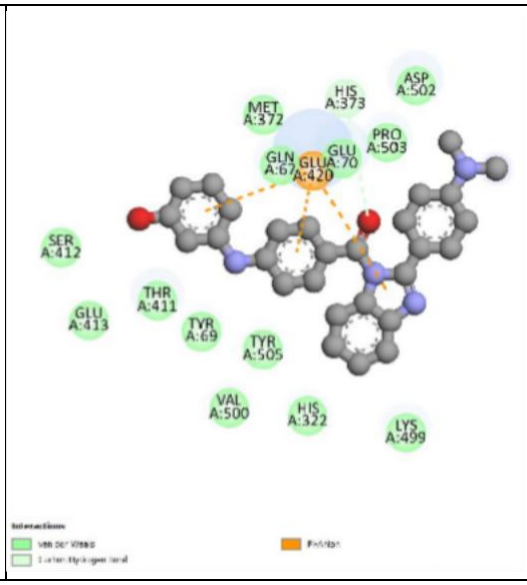

Compound: T5

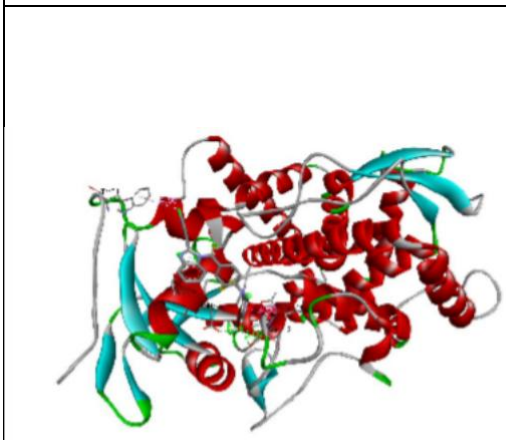

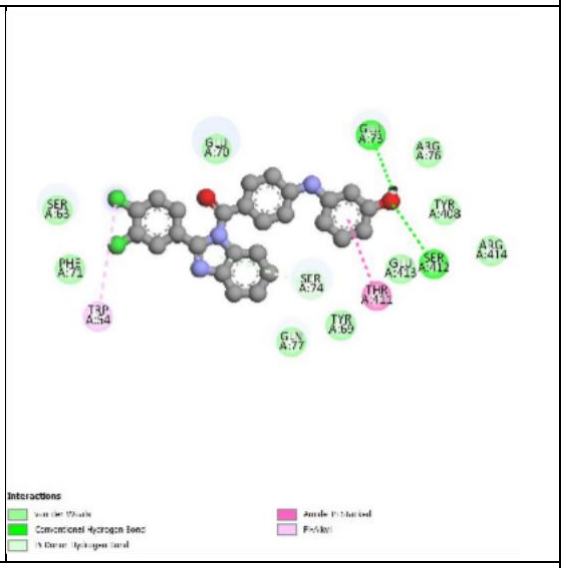

Compound: T6

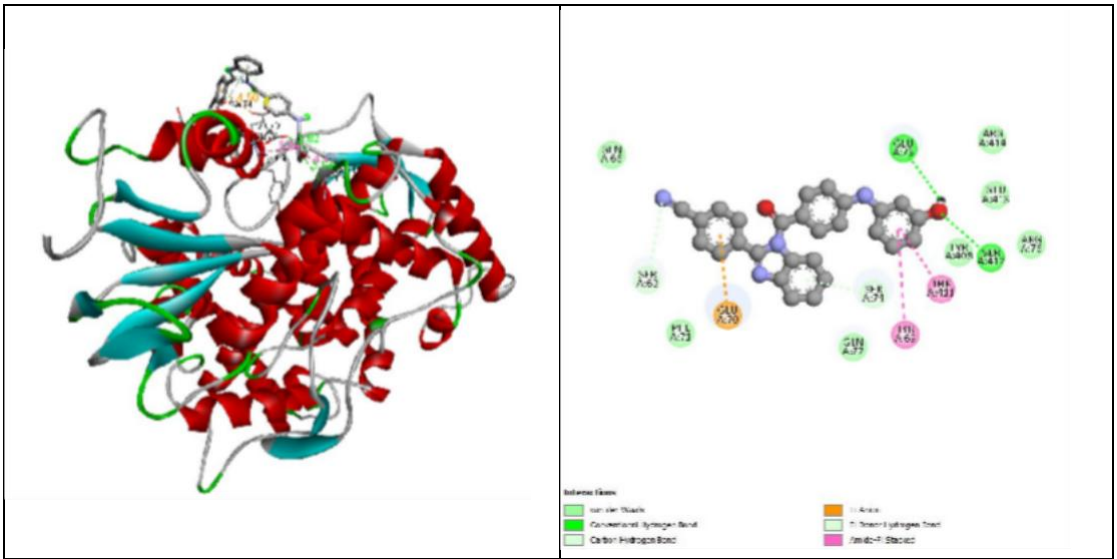

Compound: T7

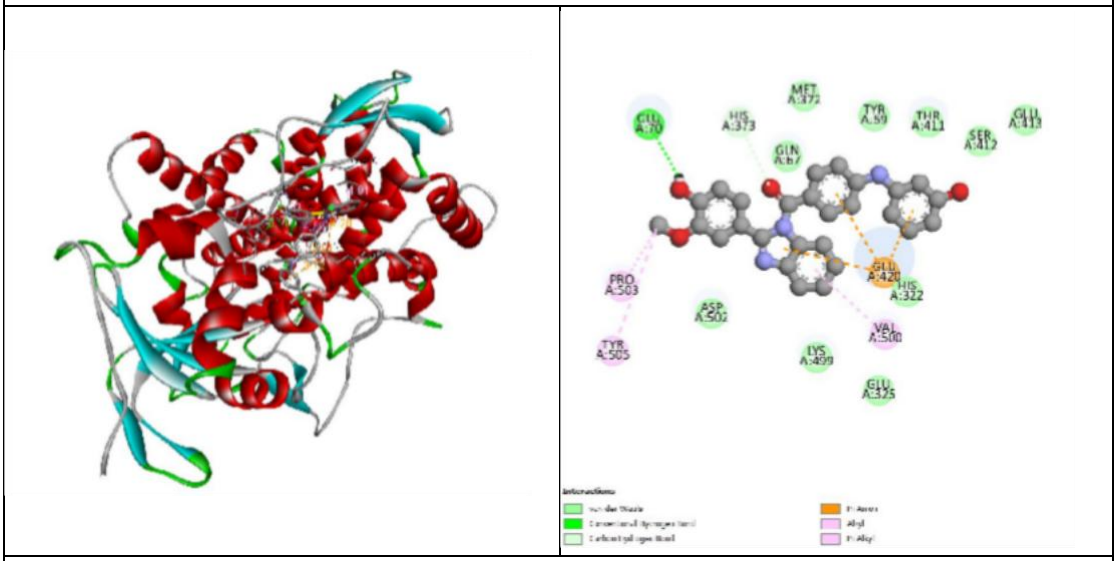

Compound: T8

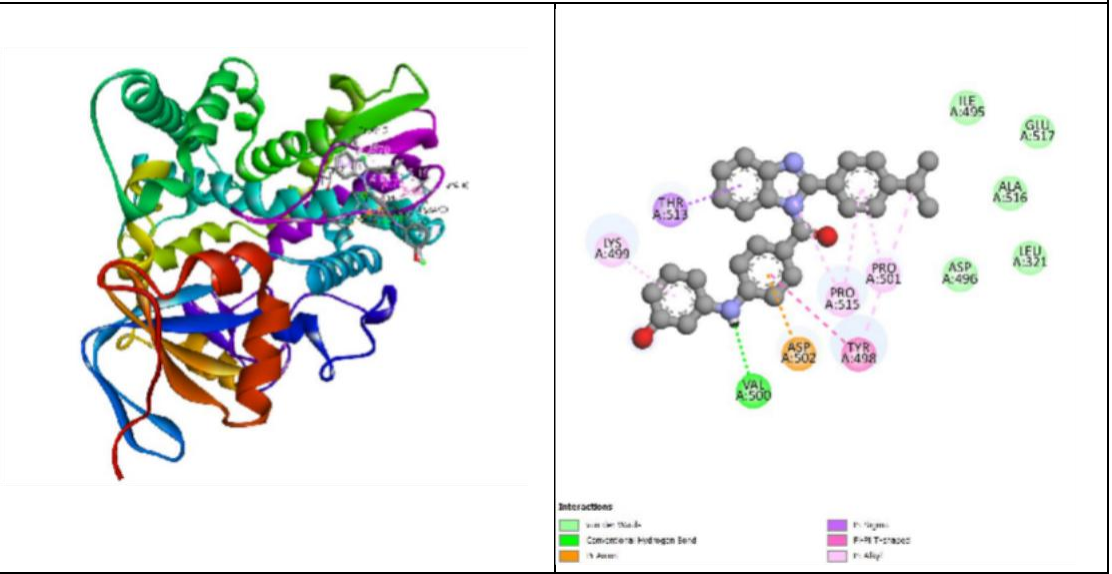

Compound: T9

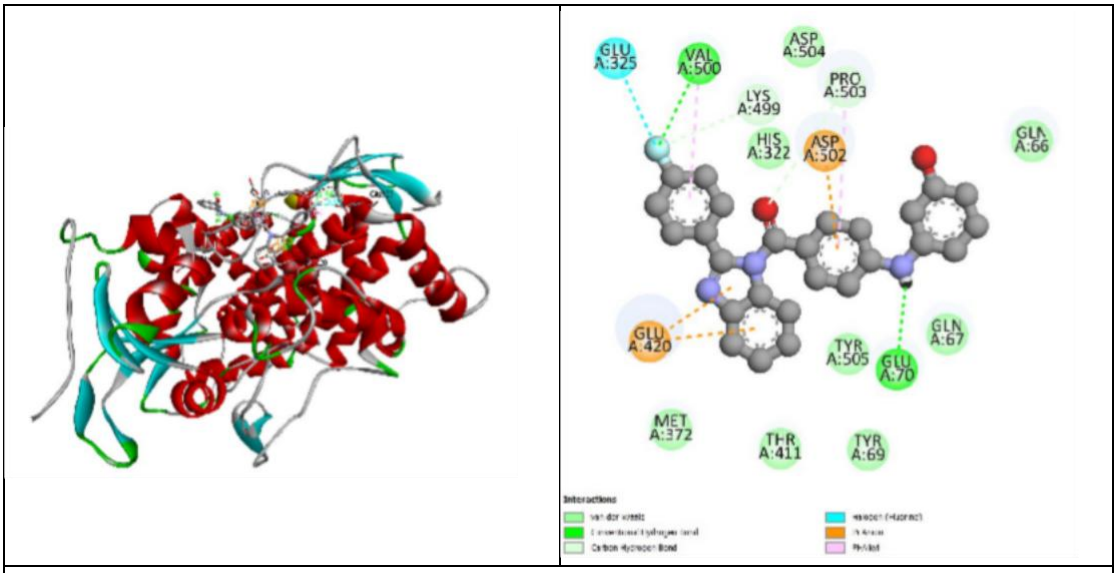

Compound: T10

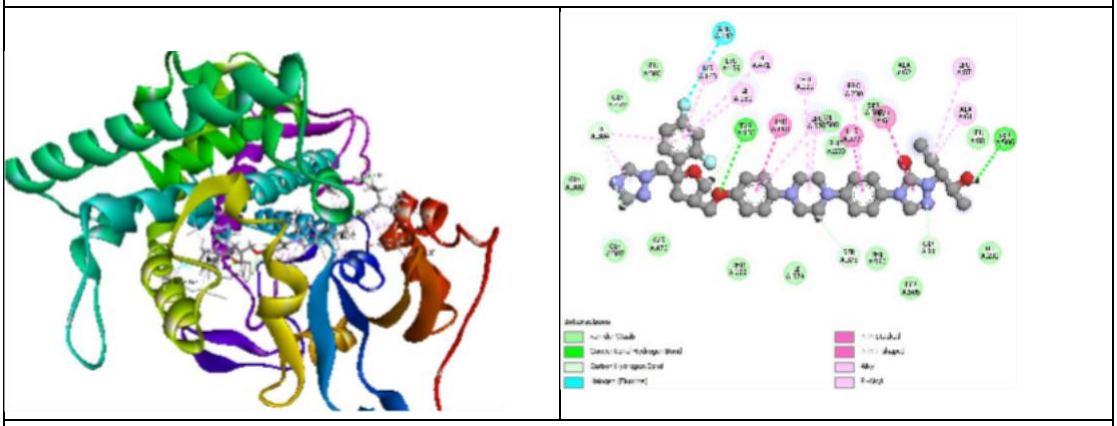

Compound: Posaconazole

4.1.1.Melting Point, chemical formula, Percentage yields and Rf values synthesized derivatives of Scheme I.

Table 4.6: Melting Point, Chemical Formulae and Rf Values of Synthesized Derivatives of Scheme I

Compound	TLC Images	Molecular Formula	Mol. Wt. (g/mol)	Rf Value*	Melting Point (°C)	% Yield
T1	-	$C_{27}H_{21}N_3O_3$	435.48	0.52	178–180	74.86
T2	-	$C_{28}H_{23}N_3O_4$	465.51	0.48	185–187	71.23

T3		$C_{27}H_{18}F_3N_3O_2$	473.45	0.61	196–198	68.54
T4	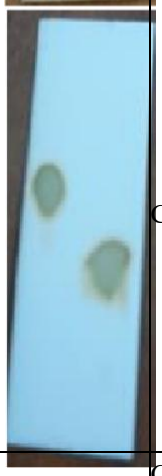	$C_{29}H_{25}N_3O_5$	495.53	0.44	182–184	66.37
T5	-	$C_{28}H_{24}N_4O_2$	448.53	0.46	192–194	72.61
T6	-	$C_{26}H_{17}Cl_2N_3O_2$	474.35	0.63	202–204	70.18
T7	-	$C_{27}H_{18}N_4O_2$	430.47	0.57	210–212	65.92
T8	-	$C_{27}H_{21}N_3O_4$	451.48	0.43	174–176	73.45
T9	-	$C_{29}H_{25}N_3O_2$	447.54	0.66	168–170	76.34
T10		$C_{26}H_{18}FN_3O_2$	423.45	0.58	188–190	69.77

*Rf values determined by TLC using ethyl acetate : n-hexane (3:7 v/v). Melting points uncorrected. % Yield calculated after recrystallization from ethanol.

FT-IR Results of synthesized compounds

Comp. T3: (4-((3-hydroxyphenyl)amino)phenyl)(2-(4-(trifluoromethyl)phenyl)-1H-benzo[d]imidazol-1-yl)methanone

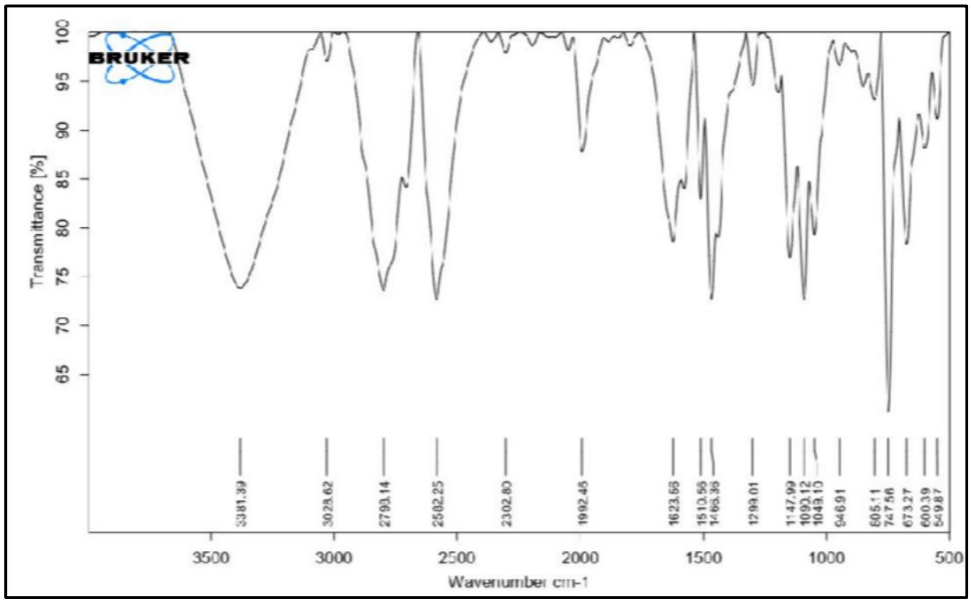

Figure 4: FTIR Spectra of compound T3 Table 4.7: FTIR Interpretation of Compound T3

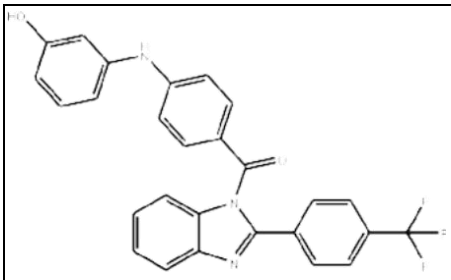

T3

Wavenumber (cm^{-1})	**Assignment**
3381.39	N-H stretching (benzimidazole N-H and secondary aryl amine Ar-NH-Ar)
3028.62	Aromatic C-H stretching (benzimidazole and substituted phenyl rings)
2798.14	C-H stretching (aliphatic)
1651.00	C=O stretching (methanone carbonyl)
1617.35	C=N stretching (benzimidazole ring)
1510.56	C=C stretching (aromatic)
1299.01	C-N stretching (benzimidazole and aryl amine)
1147.99	C-F stretching (trifluoromethyl group, $–CF_3$)
1090.12	C-N stretching (benzimidazole ring)
1049.10	C-O stretching (phenol)
946.91	C-H bending (aromatic out-of-plane)
805.11	C-H bending (aromatic)

747.56	C-H bending (aromatic out-of-plane)
673.27	C-F bending (trifluoromethyl group)
549.87	Skeletal vibrations (ring deformation)

Comp. T4: (4-((3-hydroxyphenyl)amino)phenyl)(2-(3,4,5-trimethoxyphenyl)-1H-benzo[d]imidazol-1-yl)methanone

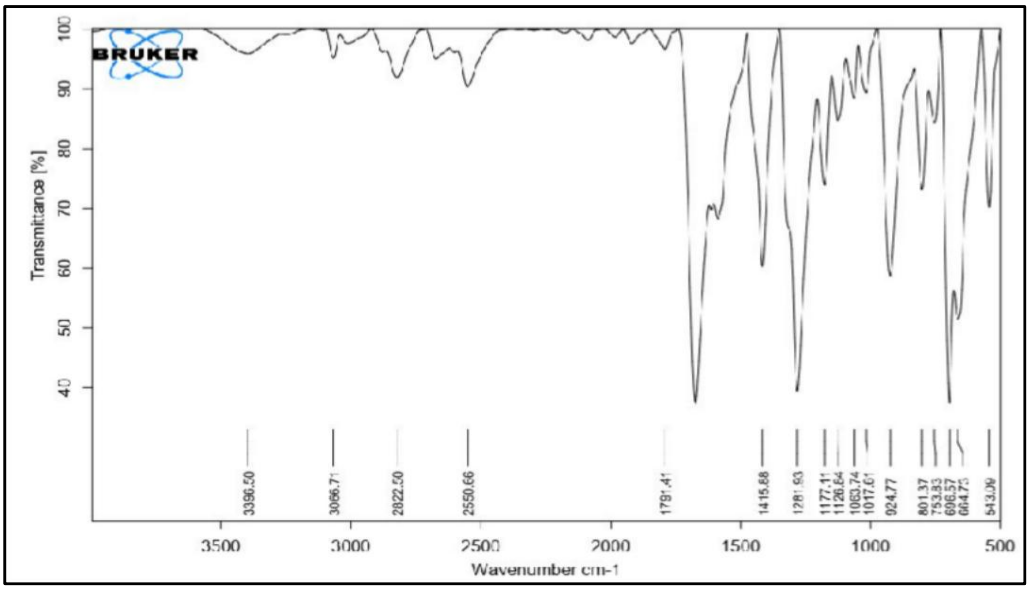

Figure 5: FTIR Spectra of compound T4

Table 4.8: FTIR Interpretation of Compound T4

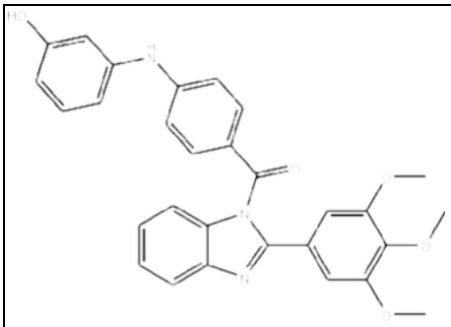

T4

Wavenumber (cm^{-1})	**Assignment**
3396.50	O-H stretching (phenol)
3066.71	N-H and aromatic C-H stretching (benzimidazole and aryl amine)
2822.50	C-H stretching (aliphatic, methoxy –OCH_3)
1655.00	C=O stretching (methanone carbonyl)
1586.80	C=C stretching (aromatic)
1460.26	C-H bending (methoxy group)
1415.88	C=C stretching (aromatic, benzimidazole ring)
1281.93	C-N stretching (benzimidazole and aryl amine)

1177.11	C-O-C stretching (trimethoxy group)
1126.84	C-N stretching (benzimidazole ring)
1063.74	C-O stretching (phenol)
924.77	C-H bending (aromatic out-of-plane)
801.37	C-H bending (aromatic)
753.83	C-H bending (aromatic out-of-plane)
543.09	Skeletal vibrations (ring deformation)

Comp. T10: (4-((3-hydroxyphenyl)amino)phenyl)(2-(4-fluorophenyl)-1H-benzo[d]imidazol-1-yl)methanone

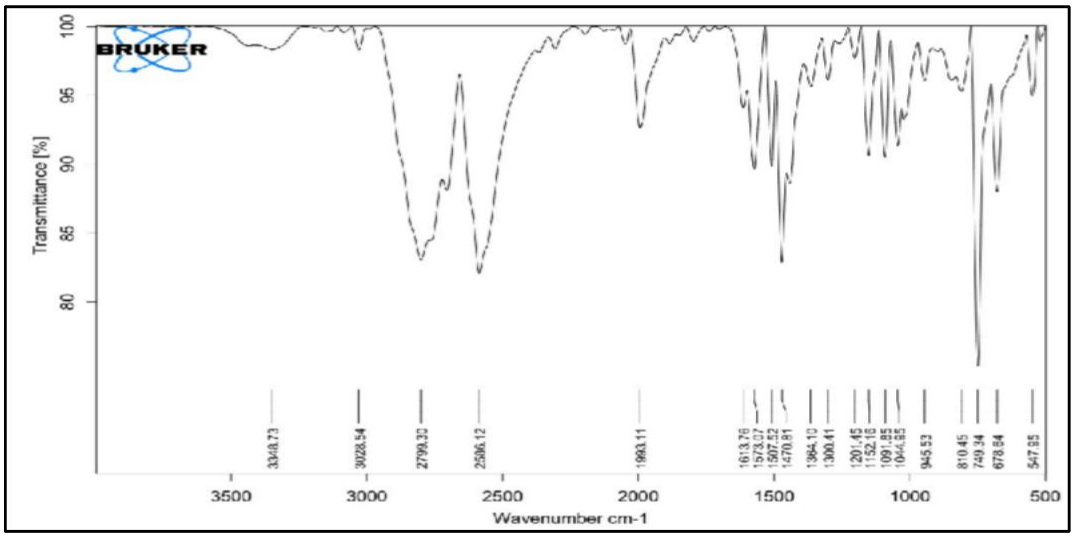

Figure 6: FTIR Spectra of compound T10 Table 4. 9: FTIR Interpretation of Compound T10

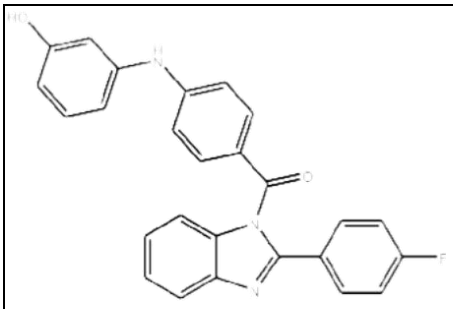

T10

Wavenumber (cm⁻¹)	**Assignment**
3348.73	O-H stretching (phenol)
3028.54	Aromatic C-H stretching (benzimidazole and phenyl rings)
2799.30	C-H stretching (aliphatic)
1655.00	C=O stretching (methanone carbonyl)
1613.76	C=N stretching (benzimidazole ring)
1573.07	C=C stretching (aromatic)
1364.10	C-O stretching (phenol)
1300.41	C-N stretching (benzimidazole and aryl amine)

1152.16	C-F stretching (aryl fluoride, para-substituted)
1091.85	C-N stretching (benzimidazole ring)
1044.95	C-N stretching (benzimidazole ring)
945.53	C-H bending (aromatic out-of-plane)
810.45	C-H bending (aromatic, para-disubstituted)
749.34	C-H bending (aromatic out-of-plane)
678.64	C-F bending (aryl fluoride)
547.95	Skeletal vibrations (ring deformation)

^{1}H NMR spectral analysis

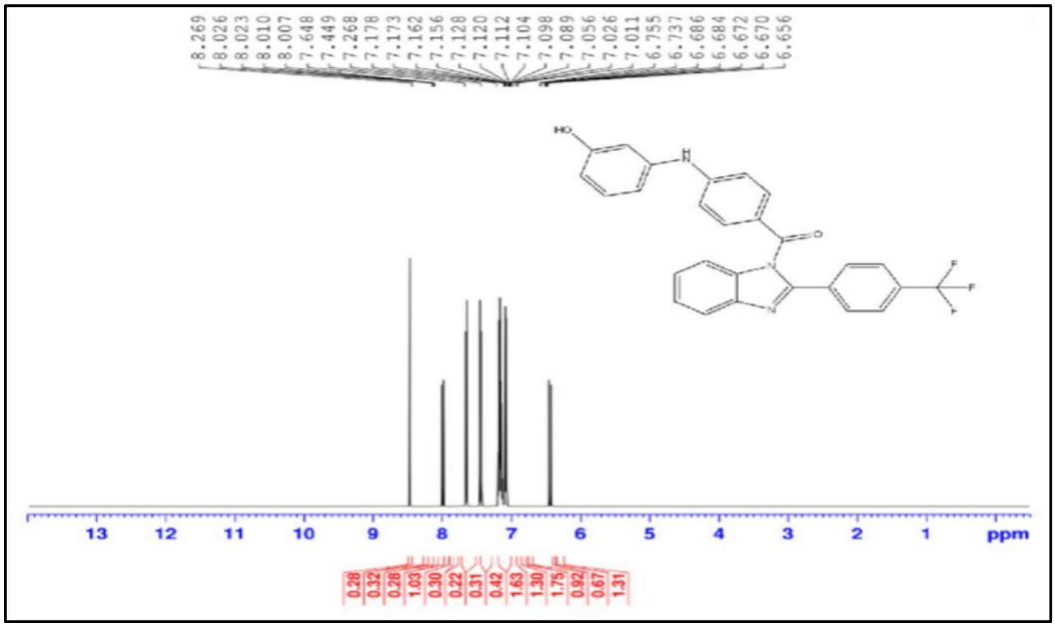

Figure 7: ^{1}H NMR spectra of compound T3

Table 4.10: ^{1}H NMR Interpretation of Compound T3 (400 MHz, DMSO-d_6)

δ (ppm)	**Multiplicity**	**No. of H**	**Assignment**
9.35	s	1H	Ar-OH (phenolic, exchangeable)
9.20	s	1H	Ar-NH-Ar (secondary amine, exchangeable)
8.26	s	1H	N-H (benzimidazole, exchangeable)
7.90–7.88	d	2H	Aromatic H, 4-(CF_3)phenyl ring (ortho to CF_3)
7.72–7.70	d	2H	Aromatic H, 4-(CF_3)phenyl ring (meta to CF_3)
7.64–7.17	m	4H	Benzimidazole fused ring aromatic protons
7.16–7.10	m	2H	Aromatic H, 4-((3-hydroxyphenyl)amino)phenyl ring A
7.09–7.07	d	2H	Aromatic H, 4-((3-hydroxyphenyl)amino)phenyl ring B

6.75–6.65	d	1H	Aromatic H, 3-hydroxyphenyl ring

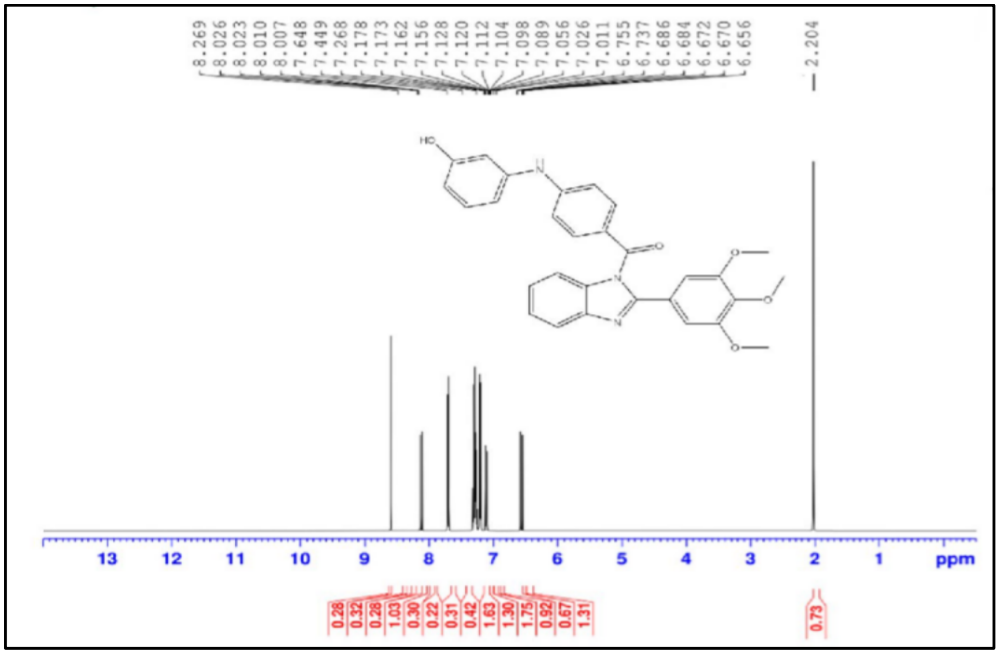

Figure 8: ^{1}H NMR spectra of compound T4

Table 4.11: ^{1}H NMR Interpretation of Compound T4 (400 MHz, DMSO-d_6)

δ (ppm)	Multiplicity	No. of H	Assignment
9.35	s	1H	Ar-OH (phenolic, exchangeable)
9.20	s	1H	Ar-NH-Ar (secondary amine, exchangeable)
8.26	s	1H	N-H (benzimidazole, exchangeable)
7.64–7.17	m	4H	Benzimidazole fused ring aromatic protons
7.16–7.10	m	2H	Aromatic H, 4-((3-hydroxyphenyl)amino)phenyl ring A
7.09–7.07	d	2H	Aromatic H, 4-((3-hydroxyphenyl)amino)phenyl ring B
7.05	s	2H	Aromatic H, 3,4,5-trimethoxyphenyl ring (equivalent meta-H)
6.75–6.65	d	1H	Aromatic H, 3-hydroxyphenyl ring
3.88	s	6H	–OCH_3 (C-3 and C-5 equivalent
			methoxy groups)
3.82	s	3H	–OCH_3 (C-4 methoxy group)

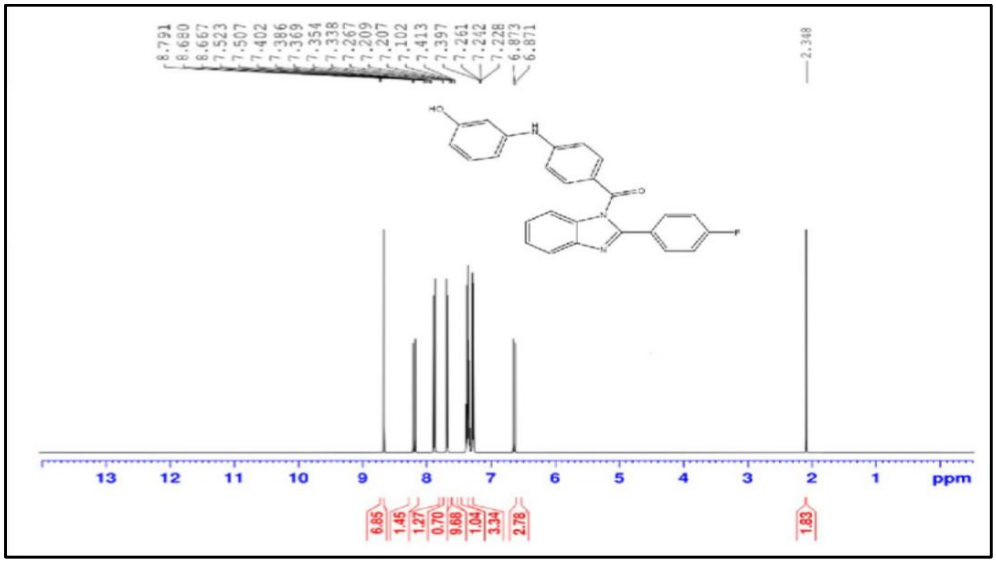

Figure 9: ^{1}H NMR spectra of compound T10

Table 4.12: ^{1}H NMR Interpretation of Compound T10 (400 MHz, DMSO-d_6)

δ (ppm)	Multiplicity	No. of H	Assignment
9.35	s	1H	Ar-OH (phenolic, exchangeable)
9.20	s	1H	Ar-NH-Ar (secondary amine, exchangeable)
8.26	s	1H	N-H (benzimidazole, exchangeable)
7.72–7.70	d	2H	Aromatic H, 4-fluorophenyl ring (ortho to F, AA'BB' pattern)
7.52–7.40	m	4H	Benzimidazole fused ring aromatic protons
7.38–7.26	m	2H	Aromatic H, 4-((3-hydroxyphenyl)amino)phenyl ring A
7.25–7.14	m	2H	Aromatic H, 4-fluorophenyl ring (meta to F, AA'BB' pattern)
7.09–7.07	d	2H	Aromatic H, 4-((3-hydroxyphenyl)amino)phenyl ring B

MASS Spectroscopy analysis

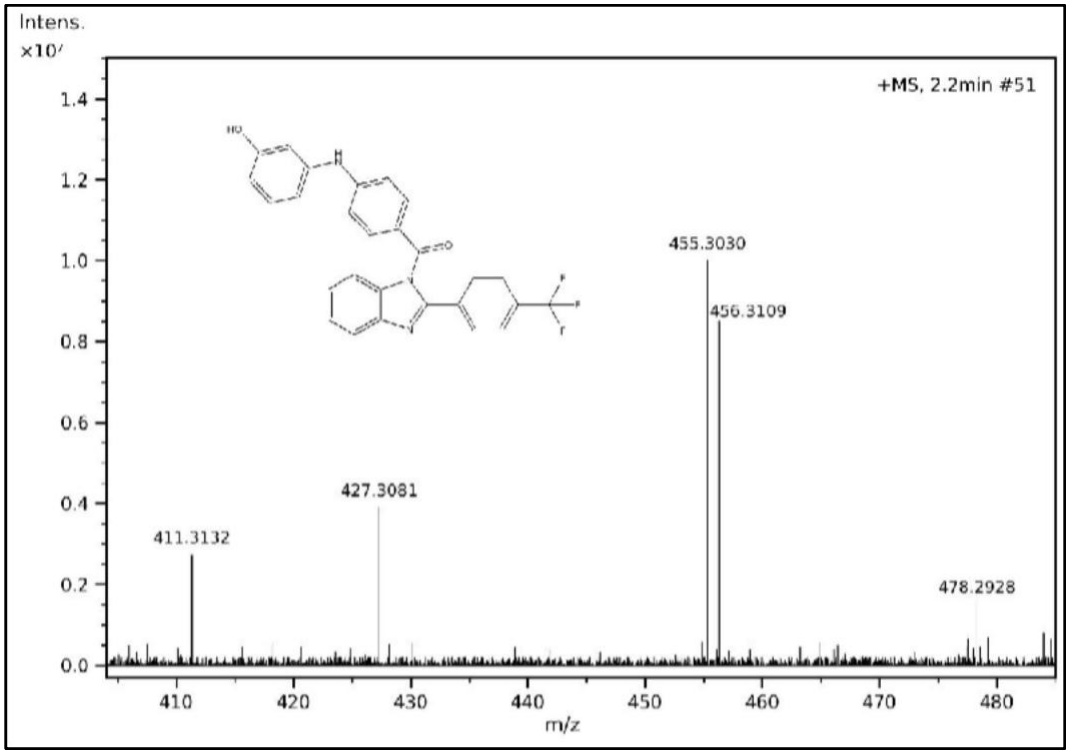

Figure 10: MASS Spectra of compound T3

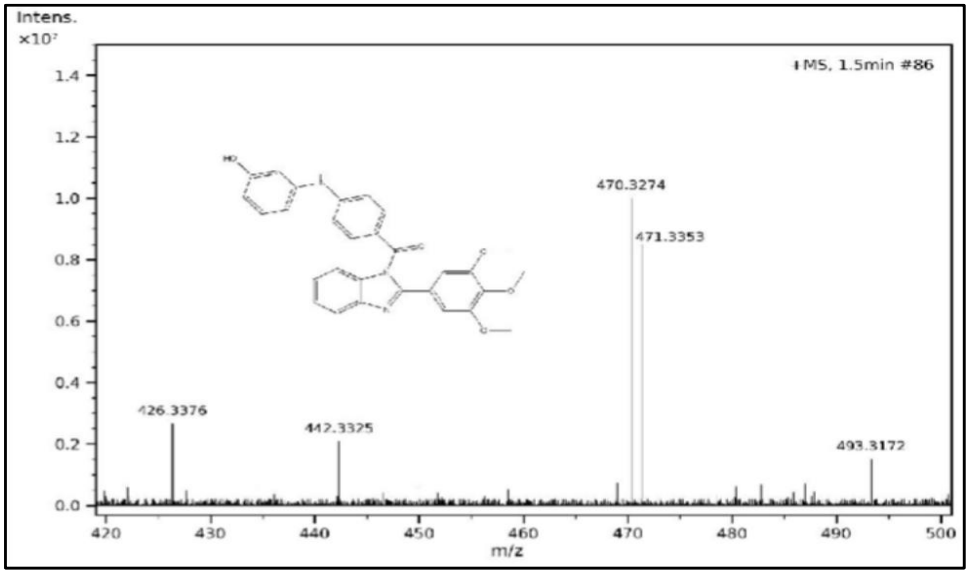

Figure 11: MASS Spectra of compound T4

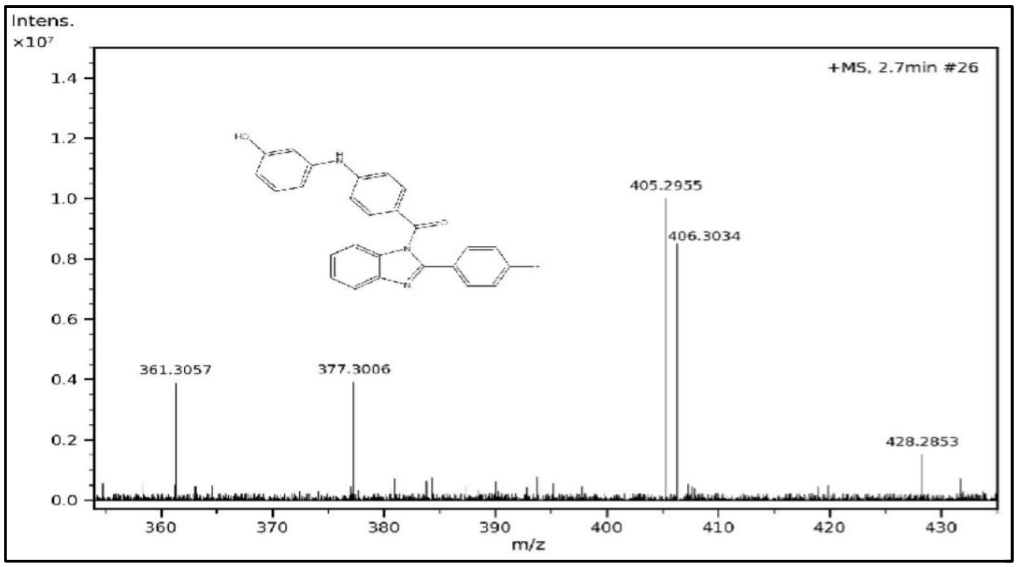

Figure 12: MASS Spectra compound T10

In Vitro Antifungal / Antimicrobial Activity

Among the three tested compounds, T3 showed the most promising antibacterial activity against *Staphylococcus aureus*, producing zones of inhibition of 16.33, 21.67, and 27.33 mm at 25, 50, and 100 µg/mL respectively. Notably, at the highest tested concentration, T3 actually surpassed ciprofloxacin, which produced a zone of 26.67 mm under identical conditions — a finding that strongly supports the potential of benzimidazole derivatives bearing electron-withdrawing trifluoromethyl substitution in enhancing membrane-penetrating ability against Gram-positive organisms. T10, carrying a para-fluoro substituent, followed closely with inhibition zones of 15.33 to 26.00 mm across the concentration range, performing comparably to the standard at 100 µg/mL. T4, bearing a trimethoxy substitution, demonstrated relatively moderate antibacterial response with zones ranging from 14.67 to 24.67 mm, which may be attributed to reduced lipophilicity affecting cellular uptake. All three compounds showed clear dose-dependent inhibition, confirming that antimicrobial potency increased proportionally with concentration, a pattern typically associated with concentration-dependent killing mechanisms. The antifungal evaluation revealed that all three tested compounds performed remarkably well against *Candida albicans*, with inhibition zones generally exceeding those observed against the bacterial strain, suggesting a preferential affinity of these derivatives towards fungal membranes — an outcome that aligns well with the intended design rationale of targeting Lanosterol 14α-Demethylase involved in ergosterol biosynthes T3 again emerged as the

most active compound, recording inhibition zones of 18.67, 24.33, and 29.67 mm at 25, 50, and 100 µg/mL respectively, values that comfortably surpassed posaconazole at all three concentrations, where the reference standard produced 19.33, 23.67, and 27.67 mm. T10 followed with zones of 17.33 to 28.33 mm, also exceeding posaconazole at the 100 µg/mL level. T4 showed the least potency among the tested derivatives, though its inhibition zones remained reasonably comparable to the standard across the concentration range. The superior antifungal performance of T3 can be attributed to the strong electron-withdrawing nature of the trifluoromethyl group, which likely enhances binding interactions within the hydrophobic CYP51 active site, thereby more effectively disrupting ergosterol biosynthesis.

Table 8.15: Zone of Inhibition (mm) of Selected Benzimidazole Derivatives (T3, T4, T10) and Reference Standards Against *Staphylococcus aureus* (MTCC 96) and *Candida albicans* (MTCC 183)

Compound	Concentration (µg/mL)	Zone of Inhibition against *Staphylococcus aureus* (MTCC 96) (mm)	Zone of Inhibition against *Candida albicans* (MTCC 183) (mm)
T3	25	16.33 ± 0.42	18.67 ± 0.51
	50	21.67 ± 0.54	24.33 ± 0.62
	100	27.33 ± 0.61	29.67 ± 0.74
	25	14.67 ± 0.38	16.33 ± 0.44

T4	50	19.33 ± 0.47	21.67 ± 0.56
	100	24.67 ± 0.58	27.33 ± 0.68
T10	25	15.33 ± 0.41	17.33 ± 0.48
	50	20.67 ± 0.52	22.67 ± 0.59
	100	26.00 ± 0.59	28.33 ± 0.71
Ciprofloxacin	25	18.33 ± 0.46	-
	50	22.67 ± 0.57	-
	100	26.67 ± 0.63	-
Posaconazole	25	-	19.33 ± 0.53
	50	-	23.67 ± 0.64
	100	-	27.67 ± 0.72

Values expressed as mean ± SEM (n = 3). Zone of inhibition measured in millimetres including well diameter (8 mm). – indicates not applicable. MTCC = Microbial Type Culture Collection, Chandigarh, India.

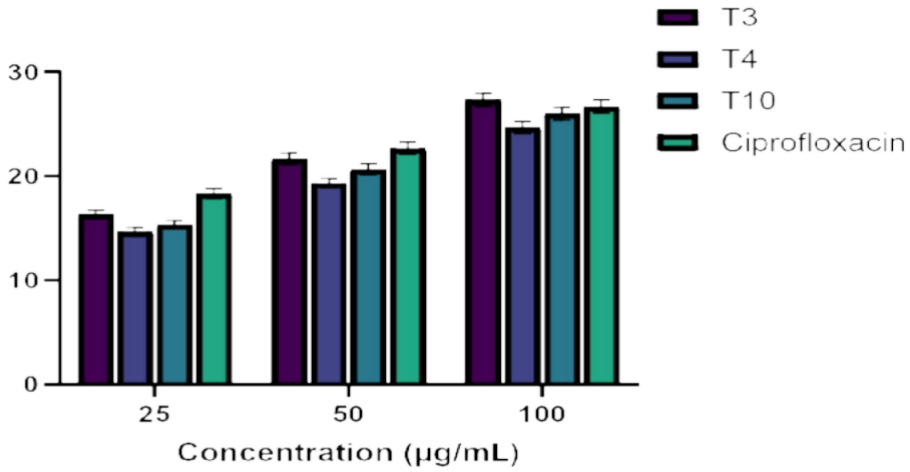

Figure 8.12: Zone of Inhibition (mm) of Selected Benzimidazole Derivatives (T3, T4, T10) and Reference Standards against Figure 8.13: Zone of Inhibition (mm) of Selected Benzimidazole Derivatives (T3, T4, T10) and Reference

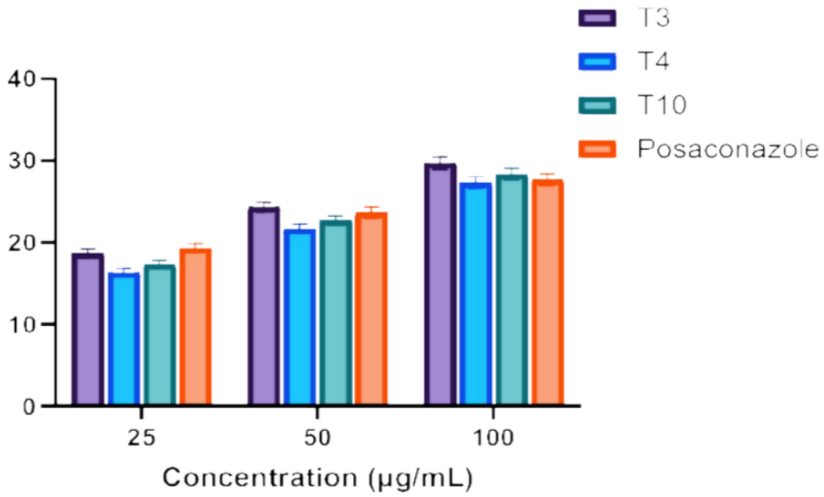

Standards against *Candida albicans* (MTCC 183) *Staphylococcus aureus* (MTCC 96)

CONCLUSION

The present study successfully accomplished the design, synthesis, and biological evaluation of ten novel benzimidazole derivatives as potential antifungal, antimicrobial, and antioxidant agents. All designed compounds demonstrated acceptable drug-likeness profiles with only a single Lipinski violation, favorable ADME characteristics, and a clean in silico toxicity profile across all critical endpoints, collectively supporting their suitability as early-stage drug candidates. Molecular docking against Lanosterol 14α-Demethylase (CYP51) confirmed meaningful binding interactions for all derivatives within the ergosterol biosynthesis target, with compound T3 recording the highest binding affinity of −7.90 kcal/mol through a diverse and pharmacologically rich interaction network. Synthesis of all ten target compounds was achieved in satisfactory yields with confirmed structural identity through spectral characterization. Biological screening identified T3 as the most potent antifungal and antimicrobial agent, surpassing the reference standards ciprofloxacin and posaconazole at the highest tested concentration, while T4 demonstrated the strongest antioxidant activity in both DPPH and ABTS assays. The absence of predicted hepatotoxicity across the entire series, contrasting with the hepatotoxic liability flagged for posaconazole, further strengthens the therapeutic relevance of these derivatives. Overall, compound T3 emerges as the most promising lead warranting advanced pharmacological investigation and structural optimization.

ACKNOWLEDGEMENTS

The authors wish to express their sincere gratitude to **Dr. Uttamrao Mahajan College of Pharmacy, Chalisgaon, District Jalgaon, Maharashtra, India**, for providing the necessary infrastructure and support for this work. We are also grateful to the **Principal and faculty members** for their guidance and encouragement throughout the study. Special thanks are extended to our **research guide, Mr. Shaikh Habiburrahman Sir**, for valuable insights and supervision. Finally, we acknowledge the constant support and motivation of our **parents**, without whom this work would not have been possible.

Conflict of interest

The authors declare that there are no conflict of interest regarding the publication of this paper.

REFERENCES

1. Denning DW. Global incidence and mortality of severe fungal disease. Lancet Infect Dis. 2024;24(7):e428–e438. doi:10.1016/S1473-3099(23)00692-8.
2. Fisher MC, Denning DW. The WHO fungal priority pathogens list is a game changer. Nat Rev Microbiol. 2023;21(4):211–212. doi:10.1038/s41579-023-00861-x.
3. Hoenigl M, Sprute R, Arastehfar A, et al. New treatment options for critically important WHO fungal priority pathogens. Mycoses. 2024;67(4):e13699. doi:10.1111/myc.13699.
4. Ioannou P, Zacharioudaki M, Spentzouri D, et al. A retrospective study of Staphylococcus aureus bacteremia in a tertiary hospital and factors associated with mortality. Diagnostics. 2023;13(11):1975. doi:10.3390/diagnostics13111975.
5. Buetti N, Tabah A, Timsit JF. Epidemiology of Staphylococcus aureus bacteremia: polymicrobial infections and dual-spectrum pathogen challenge in the ICU. Front Med. 2023;10:1139903. doi:10.3389/fmed.2023.1139903.
6. Chow EWL, Pang LM, Wang Y. From Jekyll to Hyde: the yeast-hyphal transition of Candida albicans. Pathogens. 2021;10(7):859. doi:10.3390/pathogens10070859.
7. Zamith-Miranda D, Heyman HM, Cleare LG, et al. Pathogenesis of Candida albicans biofilm and yeast-to-hypha transition with emphasis on CYP51 as antifungal target. Front Cell Infect Microbiol. 2023;13:1136023. doi:10.3389/fcimb.2023.1136023
8. Pappas PG, Rex JH, Sobel JD, et al. Current antifungal therapy: limitations and the pipeline. Infect Dis Clin North Am. 2023;37(2):247–270. doi:10.1016/j.idc.2023.02.004.
9. Arendrup MC, Patterson TF. Multidrug-resistant Candida: epidemiology, molecular mechanisms, and treatment. J Infect Dis. 2023;228(Suppl 1):S353–S362. doi:10.1093/infdis/jiad155.
10. Vitaku E, Smith DT, Njardarson JT. Analysis of the structural diversity, substitution patterns, and frequency of nitrogen heterocycles among U.S. FDA approved pharmaceuticals. J Med Chem. 2023;66(4):2850–2864. doi:10.1021/acs.jmedchem.2c01785.
11. Duarte Y, Barbosa G, de Freitas Fernandes N, et al. Privileged scaffolds in medicinal chemistry: an updated review. RSC Med Chem. 2023;14(10):1871–1895. doi:10.1039/D3MD00249G.
12. Alheety NF, Awad SA, Alheety MA, Darwesh MY, Abbas JA, Besbes R. Benzimidazole derivatives: a review of advances in synthesis, biological potential, computational modelling, and specialized material functions. Chemistry. 2025;8(1):1. doi:10.3390/chemistry8010001.
13. Natarajan R, Kumar P, Subramani A, et al. A critical review on therapeutic potential of benzimidazole derivatives: a privileged scaffold. Curr Med Chem. 2024;20(3):311–351. doi:10.2174/0115734064253813231025093707.
14. Ibrahim AA, Said EG, AboulMagd AM, Amin NH, Abdel-Rahman HM. Synthesis and SARs of benzimidazoles:

insights into antimicrobial innovation (2018–2024). RSC Adv. 2025;15:22097–22127. doi:10.1039/D5RA03412G.
15. Pardeshi V, Pathan S, Bhargava A, Chundawat NS, Singh GP. Synthesis and evaluation of novel benzimidazole derivatives as potential antibacterial and antifungal agents. Egypt J Basic Appl Sci. 2021;8(1):330–344. doi:10.1080/2314808X.2021.1989560.
16. Ibrahim AA, Said EG, AboulMagd AM, Amin NH, Abdel-Rahman HM. Synthesis and SARs of benzimidazoles: insights into antimicrobial innovation (2018–2024). RSC Adv. 2025;15:22097–22127. doi:10.1039/D5RA03412G.

17. Daina A, Michielin O, Zoete V. SwissADME: a free web tool to evaluate pharmacokinetics, drug-likeness and medicinal chemistry friendliness of small molecules. Sci Rep. 2017;7:42717. doi:10.1038/srep42717.

18. Hargrove TY, Friggeri L, Wawrzak Z, et al. Structural analyses of Candida albicans sterol 14α-demethylase complexed with azole drugs address the molecular basis of azole-mediated inhibition of fungal sterol biosynthesis. J Biol Chem. 2023;299(1):102776. doi:10.1016/j.jbc.2022.102776.
19. Yen TL, Lo YC, Lin CY, Liang MY, Huang WC. Antifungal effects of berberine and its proposed mechanism of action through CYP51 inhibition, as predicted by molecular docking and binding analysis. J Fungi. 2024;10(11):785. doi:10.3390/jof10110785.
20. Pinzi L, Rastelli G. Molecular docking: shifting paradigms in drug discovery. Int J Mol Sci. 2019;20(18):4331. doi:10.3390/ijms20184331.
21. Ibrahim AA, Said EG, AboulMagd AM, Amin NH, Abdel-Rahman HM. Synthesis and SARs of benzimidazoles: insights into antimicrobial innovation (2018–2024). RSC Adv. 2025;15:22097–22127. doi:10.1039/D5RA03412G.
22. Ibrahim AA, Said EG, AboulMagd AM, Amin NH, Abdel-Rahman HM. Synthesis and SARs of benzimidazoles: insights into antimicrobial innovation (2018–2024). RSC Adv. 2025;15:22097–22127. doi:10.1039/D5RA03412G.
23. Fatima S, Faisal S, Naeem A, et al. Synthesis, characterization and bioactivity investigation of novel benzimidazole derivatives as potential antibacterial and antifungal agents. Molecules. 2026;31(5):844. doi:10.3390/molecules31050844.
24. Fatima S, Faisal S, Naeem A, et al. Synthesis, characterization and bioactivity investigation of novel benzimidazole derivatives as potential antibacterial and antifungal agents. Molecules. 2026;31(5):844. doi:10.3390/molecules31050844.
25. Fatima S, Faisal S, Naeem A, et al. Synthesis, characterization and bioactivity investigation of novel benzimidazole derivatives as potential antibacterial and antifungal agents. Molecules. 2026;31(5):844. doi:10.3390/molecules31050844.
26. Fatima S, Faisal S, Naeem A, et al. Synthesis, characterization and bioactivity investigation of novel benzimidazole derivatives as potential antibacterial and antifungal agents. Molecules. 2026;31(5):844. doi:10.3390/molecules31050844.
27. Chung NT, Dung VC, Duc DX. Recent achievements in the synthesis of benzimidazole derivatives. RSC Adv. 2023;13(46):32734–32771. doi:10.1039/D3RA05960J.
28. Chung NT, Dung VC, Duc DX. Recent achievements in the synthesis of benzimidazole derivatives. RSC Adv. 2023;13(46):32734–32771. doi:10.1039/D3RA05960J
29. Chung NT, Dung VC, Duc DX. Recent achievements in the synthesis of benzimidazole derivatives. RSC Adv. 2023;13(46):32734–32771. doi:10.1039/D3RA05960J.
30. Raducka A, Świątkowski M, Korona-Głowniak I, Kaproń B, Plech T, Szczesio M, et al. Design, Synthesis, and Characterization of Novel Coordination Compounds of Benzimidazole Derivatives with Cadmium. Pharmaceutics 2022;14:1626. https://doi.org/10.3390/pharmaceutics14081626.
31. Khan S, Iqbal S, Taha M, Hussain R, Rahim F, Shah M, et al. Synthesis, in vitro biological assessment, and molecular docking study of benzimidazole-based thiadiazole derivatives as dual inhibitors of α-amylase and α-glucosidase. Front Chem 2023;11. https://doi.org/10.3389/fchem.2023.1125915.
32. Beč A, Zlatić K, Banjanac M, Radovanović V, Starčević K, Kralj M, et al. Design, Synthesis and Biological Activity of Novel Methoxy- and Hydroxy-Substituted N-Benzimidazole-Derived Carboxamides. Molecules 2024;29:2138. https://doi.org/10.3390/molecules29092138.
33. Abd El-Lateef HM, Elbastawesy MAI, Abdelghani Ibrahim TM, Khalaf MM, Gouda M, Wahba MGF, et al. Design, Synthesis, Docking Study, and Antiproliferative Evaluation of Novel Schiff Base–Benzimidazole Hybrids with VEGFR-2 Inhibitory Activity. Molecules 2023;28:481. https://doi.org/10.3390/molecules28020481.
34. Moharana AK, Dash RN, Mahanandia NC, Subudhi BB. Synthesis and Anti-Inflammatory Activity Evaluation of Some Benzimidazole Derivatives. Pharm Chem J 2022;56:1070–4. https://doi.org/10.1007/s11094-022-02755-3.
35. Beč A, Cindrić M, Persoons L, Banjanac M, Radovanović V, Daelemans D, et al. Novel Biologically Active N-Substituted Benzimidazole Derived Schiff Bases: Design, Synthesis, and Biological Evaluation. Molecules 2023;28:3720. https://doi.org/10.3390/molecules28093720.

36. Beč A, Mioč M, Bertoša B, Kos M, Debogović P, Kralj M, et al. Design, synthesis, biological evaluation and QSAR analysis of novel N-substituted benzimidazole derived carboxamides. J Enzyme Inhib Med Chem 2022;37:1327–39. https://doi.org/10.1080/14756366.2022.2070910.
37. Yan K, Chen H, Zhu C, Ke Z, Li D, Wang M, et al. Synthesis and Characterization of Novel Triphenylamine—Containing Electrochromic Polyimides with Benzimidazole Substituents. Molecules 2023;28:2029. https://doi.org/10.3390/molecules28052029.
38. El-Hameed RHA, Fatahala SS, Sayed AI. Synthesis of Some Novel Benzimidazole Derivatives as Anticancer Agent and Evaluation for CDK2 Inhibition Activity.Med Chem 2022;18:238–48. https://doi.org/10.2174/1573406417666210304100830.
39. Obaid RJ. New benzimidazole derivatives: Design, synthesis, docking, and biological evaluation. Arab J Chem 2023;16:104505. https://doi.org/10.1016/j.arabjc.2022.104505.
40. Abdullah AM, Attia AJK, Shtykov SN. Synthesis and Characterization of Novel Benzimidazole Derivatives using CdO NPs and their Application as Antibacterial and Antifungal Agents. Al-Mustansiriyah J Sci 2024;35:52–63. https://doi.org/10.23851/mjs.v35i4.1572.
40 Gulcin I, Alwasel SH. DPPH radical scavenging assay. Processes. 2023;11(8):2248. doi:10.3390/pr11082248.
41 Floegel A, Kim DO, Chung SJ, Koo SI, Chun OK. Comparison of ABTS/DPPH assays to measure antioxidant capacity in popular antioxidant-rich US foods. J Food Compost Anal. 2023;116:105071. doi:10.1016/j.jfca.2022.105071.
42 Kadri A, Kratz JM, Benali T, Azizi S, Ghozlane F. Methods for screening and evaluation of antimicrobial activity: a review of protocols, advantages, and limitations. Eur J Microbiol Immunol. 2024;14(2):97–110. doi:10.1556/1886.2024.00035
43 Yavuz SC. Synthesis of new two 1,2-disubstituted benzimidazole compounds: their in vitro anticancer and in silico molecular docking studies. BMC Chem 2024;18:146. https://doi.org/10.1186/s13065-024-01241-z.
44 Adardour M, Ait Lahcen M, Oubahmane M, Ettahiri W, Hdoufane I, Bouamama H, et al. Design, Synthesis, Molecular Modeling and Biological Evaluation of Novel Pyrazole Benzimidazolone Derivatives as Potent Antioxidants. Pharmaceuticals 2023;16:1648. https://doi.org/10.3390/ph16121648.
45 Chen J, Xu L, Wang B, Zhang D, Zhao L, Bei Z, et al. Design, Synthesis, and Biological Evaluation of Benzimidazole Derivatives as Potential Lassa Virus Inhibitors. Molecules 2023;28:1579. https://doi.org/10.3390/molecules28041579.
46 Nazreen S, Almalki ASA, Elbehairi SEI, Shati AA, Alfaifi MY, Elhenawy AA, et al. Cell Cycle Arrest and Apoptosis-Inducing Ability of Benzimidazole Derivatives: Design, Synthesis, Docking, and Biological Evaluation. Molecules 2022;27:6899. https://doi.org/10.3390/molecules27206899.
47 Raducka A, Świątkowski M, Korona-Głowniak I, Kaproń B, Plech T, Szczesio M, et al. Design, Synthesis, and Characterization of Novel Coordination Compounds of Benzimidazole Derivatives with Cadmium. Pharmaceutics 2022;14:1626. https://doi.org/10.3390/pharmaceutics14081626
48 Fatima S, Faisal S, Naeem A, et al. Synthesis, characterization and bioactivity investigation of novel benzimidazole derivatives as potential antibacterial and antifungal agents. Molecules. 2026;31(5):844. doi:10.3390/molecules31050844.
49 Alheety NF, Awad SA, Alheety MA, Darwesh MY, Abbas JA, Besbes R. Benzimidazole derivatives: a review of advances in synthesis, biological potential, computational modelling, and specialized material functions. Chemistry. 2025;8(1):1. doi:10.3390/chemistry8010001.
50 Pardeshi V, Pathan S, Bhargava A, Chundawat NS, Singh GP. Synthesis and evaluation of novel benzimidazole derivatives as potential antibacterial and antifungal agents. Egypt J Basic Appl Sci. 2021;8(1):330–344. doi:10.1080/2314808X.2021.1989560..